Building and Environment 301 (2026) 114596

Contents lists available at ScienceDirect

Building and Environment

journal homepage: www.elsevier.com/locate/buildenv

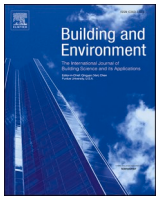

Long-term in-situ aging of HVAC filters under continuous outdoor aerosol exposure: Temporal evolution in size-resolved filtration efficiency, mass loading, pressure drop, and fan energy consumption

Chunxu Huang [a,b], Brandon E. Boor [a,b,*]

[a] Lyles School of Civil and Construction Engineering, Purdue University, West Lafayette, Indiana 47907, United States
[b] Ray W. Herrick Laboratories, Center for High Performance Buildings, Purdue University, West Lafayette, Indiana 47907, United States

ARTICLE INFO

Keywords:
HVAC filtration
Size-resolved filtration efficiency
Indoor air quality
Atmospheric aerosol particles
Fine and ultrafine particulate matter
Building ventilation systems
Outdoor/indoor air exchange

ABSTRACT

HVAC filters are a primary barrier against outdoor aerosol particles entering mechanically ventilated buildings, yet the temporal evolution of their performance under continuous outdoor aerosol exposure remains largely uncharacterized. In this study, we used a custom-built, large-scale in-situ HVAC filter aging test rig with three independently operated full-scale ventilation duct systems to conduct a two-year assessment of three full-scale filter banks comprising MERV8 pleated pre-filters paired with final-filters (MERV8 pleated, MERV13 electret bag, and MERV14 V-cell) operated at 2000 ft^3/min. Particle number size distributions from 10–10,000 nm were measured across pre- and final-filters to quantify long-term changes in size-resolved aerosol filtration efficiencies and to derive an in-situ MERV rating. Distinct aging behaviors emerged: MERV8 pre-filters exhibited substantial increases in pressure drop, enhanced efficiency as outdoor aerosol particles accumulated, and rose in-situ MERV rating (MERV8 to MERV14 after 1 year). Final-filters contributed little additional airflow resistance, but efficiency trends diverged by media type: declining for the MERV13 electret bag filter (MERV13 to MERV10 after 6.5 months), remaining stable for the MERV14 V-cell filter, and increasing for the MERV8 pleated filter (MERV8 to MERV11 after 1 year). Size-resolved outdoor aerosol measurements revealed distinct mass loading trajectories by filter type and position, with MERV8 pre-filters dominated by coarse particle accumulation and final-filters loaded predominantly by fine and ultrafine particles, with total gravimetric mass gain over two years increasing with filter MERV rating for the final-filters. Under constant airflow operation, weekly fan energy consumption increased progressively over the two-year period alongside rising filter pressure drop, with the magnitude and rate of increase varying by filter type and fan efficiency. These results demonstrate that laboratory tests of new filters alone are inadequate predictors of in-service performance and highlight the value of the in-situ MERV rating for capturing temporal evolution in filter performance. Incorporating long-term efficiency dynamics and mass loading trajectories is essential for predicting how buildings mitigate aerosol intrusion during outdoor air pollution events such as wildfires, dust storms, and smog episodes, and for optimizing filter replacement scheduling.

1. Introduction

People spend approximately 90% of their time indoors, where indoor air quality has direct consequences for both physical and psychological health [1–7]. The indoor atmosphere contains a broad spectrum of aerosol particles from both outdoor and indoor sources, including wildfire smoke, respiratory viruses, bacterial cells, fungal spores, pollen grains, sea spray aerosol, resuspended dust, tire and brake wear particles, textile fibers, nano- and microplastics, combustion and cooking aerosol, and secondary particles formed through oxidation and nucleation processes [8–22]. Numerous studies have shown that outdoor aerosol particles smaller than 2.5 μm in diameter ($PM_{2.5}$) contribute 20–90% of indoor $PM_{2.5}$ mass concentrations across the U.S., depending on building characteristics, environmental conditions, and ventilation practices [23,24]. In particular, the increasing frequency of wildfire events and the persistence of traffic-related air pollution have become major drivers of indoor aerosol particle levels, with median indoor-outdoor correlation coefficients approaching 0.9 for commercial

* Corresponding author.
E-mail address: bboor@purdue.edu (B.E. Boor).

https://doi.org/10.1016/j.buildenv.2026.114596
Received 8 December 2025; Received in revised form 23 March 2026; Accepted 7 April 2026
Available online 16 April 2026

buildings [25–27].

The building envelope provides passive protection from outdoor aerosol particles, while heating, ventilation, and air conditioning (HVAC) systems offer active mitigation through mechanical filtration [28]. Fibrous HVAC filters remain the most widely implemented air cleaning solution in buildings because they offer low cost, long service life, high removal effectiveness, and easy maintenance [29]. In contrast to oxidation-based devices, bipolar ionization systems, and ultraviolet germicidal irradiation (UVGI) technologies, which primarily inactivate biological aerosol particles and may generate undesirable by-products such as ozone and oxygenated volatile chemicals [30,31], conventional fibrous filters physically remove aerosol particles of both outdoor and indoor origin without producing secondary contaminants. Moreover, studies have shown that fibrous HVAC filters, particularly those integrated with sorbent materials, can also adsorb or decompose selected gas-phase pollutants, including ozone and certain volatile chemicals [30,31], further enhancing their advantages over alternative air cleaning technologies.

Historically, low-efficiency HVAC filters were primarily employed to protect downstream equipment from performance degradation caused by the deposition of coarse particles (>10 μm) on heat exchanger coils [32,33]. However, advances in the understanding of indoor air quality and the health implications of exposure to airborne particles have prompted widespread efforts to upgrade building HVAC systems with higher-efficiency filters capable of removing finer particles. Studies have demonstrated that sub-micron particles exhibit higher deposition rates within the human respiratory system, with the potential for deeper penetration in the lungs and increased health risks [16,18]. The recent Coronavirus Disease 2019 (COVID-19) pandemic further heightened public awareness of airborne virus transmission and underscored the critical role of HVAC filtration in mitigating disease spread. These developments have raised concerns about the energy implications of high-efficiency filters, which tend to clog more rapidly and impose higher pressure drops, necessitating greater fan power and more frequent filter replacement.

Collectively, these considerations highlight the importance of accurately evaluating HVAC filter performance to support realistic predictions of operational costs and indoor air quality outcomes. Key parameters for assessing filter performance include filtration efficiency, resistance to airflow (or pressure drop, ΔP), and dust-holding capacity (DHC). Filtration efficiency characterizes the filter's ability to remove aerosol particles, thereby improving indoor air quality and protecting occupant health. In contrast, pressure drop directly affects building energy consumption because higher pressure losses require additional fan power to maintain constant airflow in systems equipped with speed control. DHC represents the total mass of dust captured by the air filter prior to reaching the final allowable pressure drop and is therefore directly related to filter service life and replacement frequency.

The performance of HVAC filters can be experimentally evaluated using two primary approaches: (1) controlled laboratory testing and (2) in-situ (field) testing. Each method offers distinct advantages and limitations. Laboratory testing provides a highly reproducible environment in which airflow conditions, challenge aerosol characteristics, temperature, and relative humidity (RH) are tightly controlled, enabling standardized product comparisons. Such tests are indispensable for benchmarking; however, their relevance to real-world operation is limited. Most laboratory evaluations focus on small-scale filter media sheets [34–45], and studies examining full-scale HVAC filters remain comparatively rare [46,47]. Moreover, laboratory tests typically characterize only initial performance, offering little insight into how filters behave under the months- to years-long aging periods common in commercial two-stage HVAC filtration systems, where pre-filters and final-filters routinely remain in service well beyond the timescales represented in standardized test protocols, such as ANSI/ASHRAE Standard 52.2–2017 [48]. As a result, laboratory testing often fails to capture the long-term evolution of filtration efficiency, pressure drop, and mass loading (DHC) that ultimately governs real-world HVAC system performance in buildings.

Substantial discrepancies between laboratory results and in-field performance have been widely reported [49–51], driven by factors such as non-representative challenge aerosol or loading dust, unrealistic environmental parameters, and accelerated loading protocols that use artificially elevated particle concentrations [52–55]. Furthermore, current laboratory standards evaluate only the initial efficiency of new, un-aged filters and often restrict the challenge aerosol size range to 0.3–10 μm [48,56], overlooking large portions of the atmospheric aerosol size spectrum, particularly ultrafine particles (≤100 nm), which dominate outdoor and indoor number-based particle size distributions (PSDs). Electret filters pose an additional challenge, as the decay of electrostatic charges that enhance their initial capture efficiency proceeds differently in real installations than in abbreviated laboratory tests [51]. Although some methods attempt to simulate charge decay, such as ANSI/ASHRAE Standard 52.2–2017 Appendix J [48], the actual kinetics and resulting performance impacts remain insufficiently characterized.

In-situ testing, by contrast, evaluates filters within operating HVAC systems under authentic indoor-outdoor environmental conditions. Real-world temperature, RH, airflow patterns, and ambient aerosol composition are inherently captured, and interactions among filter media, ductwork, and fan systems are preserved. As a result, in-situ testing mitigates limitations of laboratory methods and provides a realistic assessment of long-term filter performance, loading behavior, and operational energy implications.

Historically, in-situ studies have offered only a limited view of HVAC filter behavior because most investigations examined new or lightly aged filters, despite the fact that pre-filters in commercial two-stage HVAC filtration systems are often operated for many months and final-filters may remain in service for multiple years before replacement. As a result, previous work largely overlooked how filtration efficiency and resistance to airflow evolve as particles accumulate on filter media over extended periods. Stephens et al. (2013) evaluated newly installed HVAC filters in real buildings and found substantial variability in initial efficiency among filters with the same nominal rating, demonstrating that laboratory evaluations do not consistently reflect field performance [57]. Similarly, Fazli et al. (2019) examined fine and ultrafine particle removal by new residential filters but did not assess temporal changes in efficiency [58]. Extended-duration in-situ evaluations remain scarce due to the labor- and time-intensive nature of field monitoring over months or years. In two such studies, Li et al. (2019) and Alavy et al. (2020) tracked residential filters (MERV8–14) for three months and observed declining efficiency in electret filters, while mechanical (non-electret) filters showed comparatively stable performance [59,60]. Additional work has shown that increases in filter pressure drop during loading elevate fan energy consumption in constant-airflow systems equipped with speed control, underscoring the operational energy penalties associated with long-term filter use [61]. In contrast, in systems with constant-speed fans, higher filter ΔP can reduce energy use by lowering volumetric airflow rates. However, the resulting decrease in airflow under higher ΔP conditions also reduces the amount of filtered air supplied indoors, which can diminish indoor air quality [61,62]. Evaluating the temporal progression of filter ΔP is therefore essential for understanding long-term HVAC energy performance and its implications for both building energy consumption and indoor air quality [61,62].

The present study reports a two-year (112-week) in-situ evaluation of HVAC filter performance under continuous outdoor aerosol exposure using a custom-designed, full-scale filter aging test rig consisting of three independently speed-controlled ventilation ducts operated at a constant airflow rate setpoint. To the authors' knowledge, this is the first in-situ investigation to obtain continuous, size-resolved measurements of outdoor aerosol particles both upstream and downstream of pre- and final-filter stages throughout the entire loading period The objectives of this work are to characterize long-term changes in: (1) filtration performance, including size-resolved filtration efficiency and a newly

developed in-situ MERV rating, and (2) resistance to airflow (filter pressure drop, ΔP), size-resolved filter mass loading, and the associated fan energy consumption under constant airflow operation as filters age under extended service. The filtration bank consisted of MERV8 pleated pre-filters paired with MERV8 pleated, MERV13 electret bag, or MERV14 V-cell final-filters, enabling comparison across multiple efficiency classes within the same HVAC system. The resulting continuous dataset provides a uniquely comprehensive reference for understanding the coupled dynamics of filter loading, evolving efficiency, and pressure drop growth under real-world outdoor aerosol aging conditions. This work, conducted as part of ASHRAE RP-1734, supports the development of the forthcoming ASHRAE Guideline 35, *Method for Determining the Energy Consumption Caused by Air-Cleaning and Filtration Devices*, and advances the modeling and prediction of long-term HVAC filter performance in mechanically ventilated buildings.

2. Materials and methods

2.1. Custom-built, large-scale in-situ HVAC filter aging test rig

Fig. 1 presents a schematic and photographs of the full-scale in-situ HVAC filter aging test rig located at the Ray W. Herrick Laboratories in West Lafayette, IN, U.S. The rig was custom-designed and built to meet the requirements of ASHRAE RP-1734 and to provide a controlled platform for multi-year, uninterrupted aging of HVAC filters. It consists of three independently controlled full-scale ventilation ducts that allow simultaneous aging of three pre-filter/final-filter configurations. The test rig is 32 ft long with a nominal 2 × 2 ft cross-section and is partitioned into Duct 1, Duct 2, and Duct 3 (Fig. 1). These ducts contain the following filter combinations: Duct 1: MERV8 pleated pre-filter and MERV14 V-cell final-filter; Duct 2: MERV8 pleated pre-filter and MERV13 electret bag final-filter; Duct 3: MERV8 pleated pre-filter and

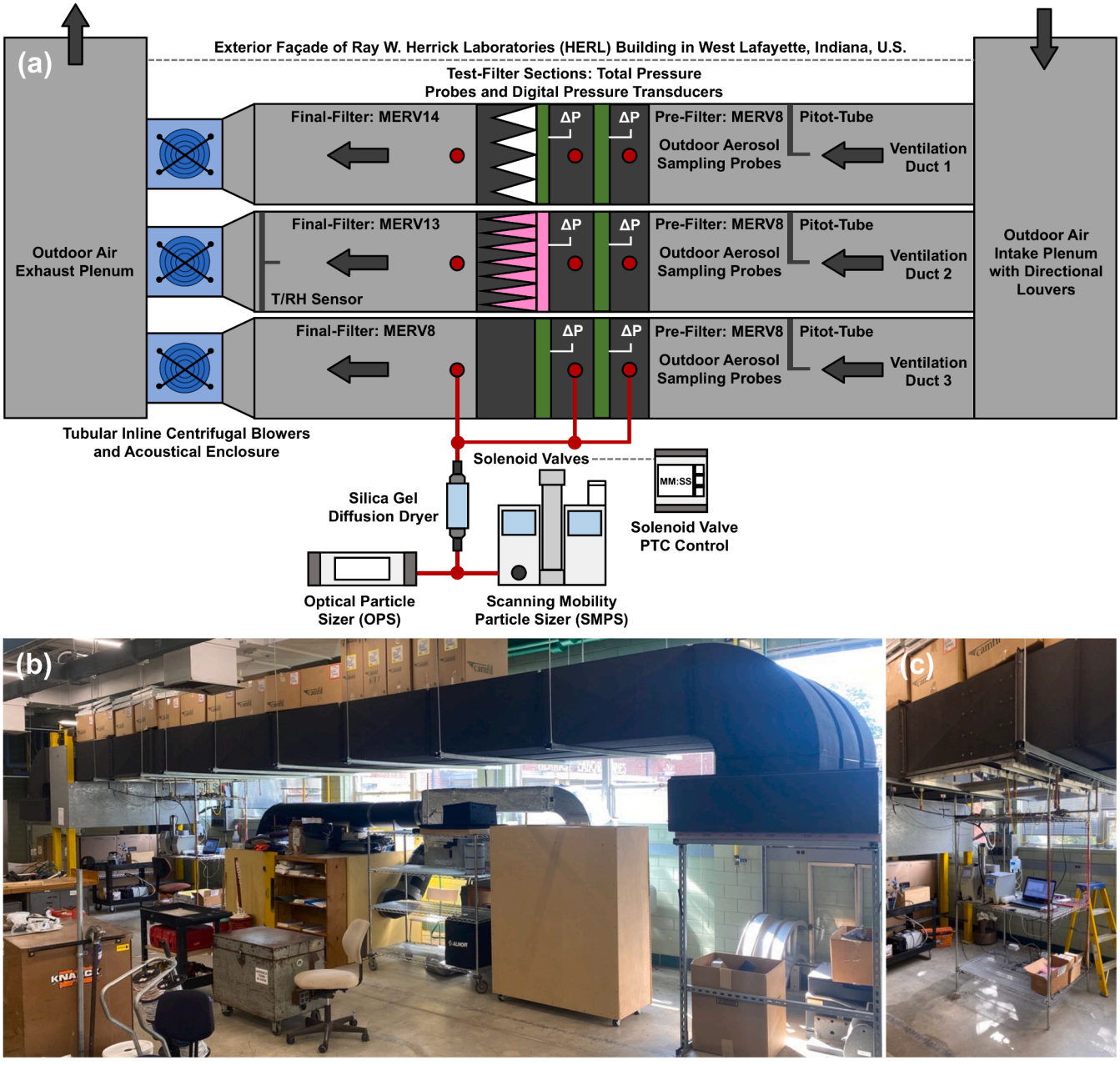

Fig. 1. Full-scale in-situ HVAC filter aging test rig located at the Ray W. Herrick Laboratories in West Lafayette, IN, U.S.: (a) schematic of the three-duct ventilation system and measurement instrumentation; (b-c) photographs of the installed test rig.

MERV8 pleated final-filter. The system is installed indoors adjacent to the building's exterior façade, enabling direct intake of unconditioned outdoor air for real-world outdoor aerosol loading. Each duct is equipped with a downstream tubular inline centrifugal blower controlled by a variable frequency drive (VFD), which draws outdoor air through the system and exposes filters to authentic meteorological variability (temperature, RH, and precipitation) throughout the long-term aging experiment. All blowers are enclosed within a custom-built acoustic housing to minimize interior noise intrusion during the continuous, multi-year operation of the test rig.

Outdoor air enters through a common intake plenum and is distributed to the three parallel ducts using internal directional louvers. Outdoor aerosol-laden airflow then passes through the filter bank, where the installed filters capture outdoor aerosol particles over time. The centrifugal blowers were specified to deliver a constant volumetric airflow of 2000 ft^3 min^{-1} against a design static pressure of 5 in H_2O, accommodating the maximum anticipated end-of-life resistance of the filters in addition to duct surface roughness. After passing through the filters, the airflow is exhausted back outdoors through a plenum.

Notably, formal qualification tests such as aerosol uniformity profiling were not part of the initial design criteria. However, to ensure data reliability, we cross-validated our initial pressure drop measurements against data from ANSI/ASHRAE Standard 52.2–2017-compliant laboratories. As shown in Table S2, our measurements show strong agreement with certified laboratory results at the same volumetric airflow rates. This agreement confirms that, despite the absence of formal standard qualification, the data generated by our test rig are consistent with those obtained from ANSI/ASHRAE Standard 52.2–2017-compliant laboratory facilities.

2.2. HVAC filter selection

Three types of HVAC filters were selected for this study in accordance with ASHRAE RP-1734 requirements. All filters had a nominal cross-sectional area of 24 × 24 inches but differed in thickness, media composition, and construction (Table 1). The MERV8 filters were 2-inch pleated panel filters composed of a proprietary blend of mechanical filtration fibers without electret charging. The MERV13 filters were eight-pocket bag filters, each pocket 30 inches deep, fabricated from an electrostatically enhanced synthetic microfiber media. The MERV14 filters were 12-inch-deep mini-pleated V-bank box filters constructed from microfine glass fiber media.

Each test duct employed a two-stage filtration configuration in which a MERV8 pre-filter was installed upstream of the MERV8, MERV13, or MERV14 final-filter. The pre-filter removed coarse particles (>1 μm), thereby preventing premature loading and clogging of the downstream final-filters. This follows standard HVAC practice, which extends final-filter service life, stabilizes airflow, and reduces replacement costs. The two-stage configuration also enabled the present study to isolate and evaluate the performance evolution of the final-filters for sub-micron particles (≤1 μm), which dominate the number-based PSDs in both outdoor and indoor atmospheric environments [52,58]. This arrangement additionally provides empirical reference data to support the forthcoming ASHRAE Guideline 35, which will focus on accelerated loading of HVAC filters using a sub-micron potassium chloride (KCl) aerosol.

2.3. Experimental protocol

The in-situ HVAC filter aging experiment began in November 2020 and concluded in February 2023, spanning a total of 112 weeks. Prior to installation, each filter was weighed outdoors to ensure that initial mass measurements reflected the environmental conditions to which the filters would subsequently be exposed. After gravimetric characterization, each filter was installed in its respective filter bank with all edges carefully sealed to minimize bypass leakage. The blower for each duct was then activated and adjusted via the VFD to establish a nominal volumetric airflow rate of 2000 ft^3 min^{-1}. Because increases in filter pressure drop from aerosol loading are minimal over short time intervals, the VFD was manually readjusted once per week to maintain the 2000 ft^3 min^{-1} setpoint. Concurrently, aerosol instruments collected number-based PSDs for subsequent filtration efficiency calculations.

At the approximate midpoint of the study (60 weeks), the three MERV8 pre-filters were replaced with identical units to prevent excessive resistance on the blowers. The final-filters remained in place, allowing aging to continue for a second full year under realistic outdoor aerosol exposure. This procedure mirrors standard HVAC maintenance protocols, in which pre-filters are routinely replaced while final-filters remain in service. The resulting data capture the dynamic fluctuations in final-filter loading that occur in real building environments when pre-filters are periodically replaced. At the conclusion of the 112-week period, all filters were removed and re-weighed outdoors to determine the total mass of outdoor aerosol particles accumulated on each filter over the course of the aging experiment.

2.4. Instrumentation and system control

2.4.1. Measurement of volumetric airflow rate in the in-situ test rig

Volumetric airflow rate measurements were obtained using pitot-tubes (Model 160, Dwyer Instruments LLC, Michigan City, IN, U.S.), differential pressure transducers (Model 265, Setra Systems Inc., Boxborough, MA, U.S.), and a data acquisition (DAQ) system (Model 6211, National Instruments Inc., Austin, TX, U.S.) controlled through LabVIEW (Version 2020, National Instruments Inc., Austin, TX, U.S.) (Table 2). A temperature and RH transmitter (Model SRH200, Setra Systems Inc., Boxborough, MA, U.S.) was installed downstream of the final-filter in one of the ventilation ducts to continuously record the thermodynamic properties of the airflow, enabling calculation of the air density. The pitot-tube in each test duct measured velocity pressure, which was converted by the pressure transducers into analog voltage signals. These signals were collected by the DAQ system, which calculated instantaneous volumetric airflow rates based on velocity pressure and air density. A single pitot-tube was mounted 2 ft upstream of each pre-filter, a location selected through preliminary air velocity profile assessments that identified this region as having the most stable and uniform airflow across the duct cross-section.

Maintaining airflow near the target value of 2000 ft^3 min^{-1} was essential, as a primary objective of the study was to compare filter aging under consistent operating conditions. To determine the true average duct airflow, a weekly pitot-tube traverse was performed following ANSI/ASHRAE Standard 41.2–2022 [63]. A correction factor was then derived as the ratio of the traverse-based average airflow to the airflow

Table 1
Specifications of the HVAC filters evaluated in the in-situ outdoor aerosol aging study.

Filter Type	Filter Configuration	Nominal Size (HxWxD) (in)	Filter Media Area (ft^2)	Media Type	Electret Filter?	Nominal Initial Filter ΔP (Pa / in H_2O)	Recommended Final Filter ΔP (Pa / in H_2O)
MERV8	Pleated Panel Filter	24 × 24 × 2	17.3	Synthetic Blend of Polyester Media	No	77.1 / 0.31	248.8 / 1.0
MERV13	Multi-Pocket Bag Filter	24 × 24 × 30	81	Blend of Synthetic Microfibers	Yes	87.1 / 0.35	2X Initial Filter ΔP
MERV14	Mini-Pleated V-Bank Box Filter	24 × 24 × 12	200	Microfine Glass Fibers with an Acrylic Resin Binder	No	84.6 / 0.34	373.3 / 1.5

Table 2
Description of instrumentation used in the in-situ HVAC filter aging test rig.

Instrument	Manufacturer	Model	Accuracy	Range	Function
Pressure Transducers	Setra Systems Inc.	Model 265	±0.25% ±0.25%	0 to 5 in H_2O 0 to 0.5 in H_2O	Differential pressure transducer for filter ΔP measurement Differential pressure transducer for volumetric airflow rate measurement
Temperature & RH Transmitter	Setra Systems Inc.	Model SRH200	±2.5% RH ±0.3 °C	0 to 100% RH −40 to 60 °C	Sensor for monitoring in-duct temperature and RH
Pitot-Tubes	Dwyer Instruments LLC	Model 160	±2 to 5%	400 to 20,000 ft min^{-1}	Air velocity measurement
Data Acquisition Board	National Instruments Inc.	Model 6211	±2.69 mV	AO/I: ±10 V	Data acquisition for voltage signals and control
OPS	TSI Inc.	Model 3330	-	300 to 10,000 nm	Aerosol number-based PSD measurement (optical diameter, D_o)
SMPS	TSI Inc.	Model 3938NL88 Model 3910	-	10 to 500 nm with long DMA 10 to 300 nm with radial DMA	Aerosol number-based PSD measurement (electrical mobility diameter, D_{em})
PTC	OMEGA Engineering Inc.	Model PTC-15	-	0.1 s to 99 min 59 s	Controls solenoid valves for aerosol sampling location switching
Precision Balance	OHAUS Corporation	Model AX8201/E	±0.1 g	0 to 8200 g	Filter mass measurement

measured at the fixed pitot-tube height. An example traverse profile is shown in Figure S1. Because only a single pitot-tube reading was collected continuously throughout the 112-week experiment, this correction factor was updated weekly as part of the quality-control protocol to ensure accurate airflow measurement over the multi-year testing period.

2.4.2. Measurement of HVAC filter pressure drop in the in-situ test rig

The configuration for filter ΔP measurement is shown in Fig. 1. Pressure drops across each pre-filter and final-filter were measured using total pressure probes rather than static pressure taps to account for potential localized increases in air velocity immediately downstream of the filter media caused by reductions in effective cross-sectional area. Digital differential pressure transducers (Series 265, Setra Systems Inc., Boxborough, MA, U.S.) continuously monitored ΔP across each pre-filter and final-filter stage throughout the study (Table 2). Prior to the start of the in-situ aging experiment, all pressure transducers were calibrated against a high-precision differential pressure gauge (DG-500, The Energy Conservatory, Minneapolis, MN, U.S.) to ensure measurement accuracy. Six transducers were dedicated to filter ΔP measurements (three for pre-filters and three for final-filters), and an additional three transducers were used in conjunction with pitot-tubes for volumetric airflow rate measurements. This configuration enabled continuous, high-resolution tracking of pressure drop evolution as the filters accumulated outdoor aerosol over the 112-week testing period.

2.4.3. Measurement of outdoor aerosol size distributions in the in-situ test rig

A scanning mobility particle sizer (SMPS; Model 3938NL88, TSI Inc., Shoreview, MN, U.S.) and an optical particle sizer (OPS; Model 3330, TSI Inc., Shoreview, MN, U.S.) were used to measure number-based PSDs upstream and downstream of each pre- and final-filter. The SMPS consisted of a Kr-85 bipolar charger (370 MBq; Model 3077A, TSI Inc., Shoreview, MN, U.S.), a long differential mobility analyzer (DMA; Model 3081, TSI Inc., Shoreview, MN, U.S.), and a water-based condensation particle counter (CPC; Model 3788, TSI Inc., Shoreview, MN, U.S.) (Table 2). Outdoor aerosol particles were charged to a known equilibrium distribution, size-classified by their electrical mobility in the DMA, and subsequently counted by the CPC. The SMPS measured particles from 10–500 nm electrical mobility diameter (D_{em}) with a 2-min scan time. Number-based PSDs ($dN/dlogD_{em}$; cm^{-3}) were extracted using the data acquisition software from the manufacturer (Aerosol Instrument Manager, TSI Inc., Shoreview, MN, U.S.). Periodically, when the primary SMPS was unavailable due to maintenance or use in concurrent laboratory experiments, a portable SMPS (Model 3910, TSI Inc., Shoreview, MN, U.S.) was deployed as a substitute; it provided comparable PSDs from D_{em} = 10–300 nm using a unipolar charger and a radial DMA.

The OPS was used to measure number-based PSDs for particles characterized by their optical diameter (D_o) derived from single-particle light scattering. Number-based PSDs ($dN/dlogD_o$; cm^{-3}) were obtained for particles with D_o = 300–10,000 nm. The OPS operates by directing a focused laser beam into the sensing volume; as individual particles traverse the beam, the resulting scattered-light pulses are detected and converted into particle counts and size estimates. Reported D_o values assume spherical particles with a dynamic shape factor of unity, which differs fundamentally from the electrical mobility-based sizing of the SMPS. Consequently, variations in particle refractive index and morphology may influence the measured PSDs by the OPS. During the two-year measurement campaign in the in-situ test rig, the OPS experienced periodic internal pump malfunctions that required maintenance; these interruptions resulted in several short gaps in the optical-based PSD dataset.

Data from the SMPS and OPS were merged to obtain continuous number-based PSDs ($dN/dlogD_{em(o)}$; cm^{-3}) across the full measured size range from $D_{em(o)}$ = 10–10,000 nm, following previously established methods for combining multimodal aerosol measurements [64,65]. An interpolation procedure was applied within the overlapping region ($D_{em(o)}$ = 300–500 nm) to ensure a smooth transition between electrical mobility- and optical-based particle sizing. This approach has been validated in prior aerosol research and provides a robust basis for constructing unified PSDs from multiple instruments [14]. Merged number-based PSDs were converted to surface area- ($dS/dlogD_{em(o)}$; μm^2 cm^{-3}), volume- ($dV/dlogD_{em(o)}$; μm^3 cm^{-3}), and mass-based ($dM/dlogD_{em(o)}$; μg m^{-3}) PSDs following methods in [14].

The multi-location outdoor aerosol sampling configuration is shown in Fig. 1. Outdoor aerosol PSD measurements were collected at three locations in each ventilation duct: (1) upstream of the MERV8 pre-filter, (2) downstream of the pre-filter (upstream of the final-filter), and (3) downstream of the final-filter. Because only one SMPS and one OPS were available, particle sampling was sequentially cycled among the three locations using a programmable timing controller (PTC; Model PTC-15, OMEGA Engineering Inc., Norwalk, CT, U.S.) coupled to a set of solenoid valves. Likewise, aerosol sampling was performed in only one ventilation duct per week, with the sampling manifold manually repositioned to the next duct each week. The timer switching interval was set to 4 min, and both instruments operated with 2-min scan durations; the first scan following each switch was discarded to avoid transient switching artifacts. To minimize RH effects and ensure consistency across measurements, outdoor aerosol samples were dried using a silica gel diffuser

dryer (Model 3062, TSI Inc., Shoreview, MN, U.S.) prior to entering the SMPS and OPS. The desiccant was replaced weekly, and zero checks were performed after each replacement. Additionally, aerosol sampling lines were cleaned and inspected weekly, and all aerosol instruments were routinely checked for operational stability and potential malfunctions.

2.5. HVAC filter performance metrics

The pressure drop (ΔP) across each pre- and final-filter was recorded continuously at 1 Hz using the LabVIEW-based DAQ system to quantify the impact of filter aging on airflow resistance under the constant volumetric flow rate of 2000 $ft^3\ min^{-1}$. Initial and final filter masses, measured gravimetrically outdoors, were used to determine the total mass of outdoor aerosol particles accumulated on each filter over the 112-week aging period. These measurements provided a direct assessment of long-term outdoor aerosol loading behavior across the three filtration configurations in the in-situ test rig.

The fan energy consumption associated with the pressure drop across each pre-filter and final-filter was estimated following Eurovent 4/21–2019 [66,67], as given by Eq. (1):

$$W = \frac{Q \cdot \Delta P \cdot t}{\eta_{fan} \cdot 1000} \quad (1)$$

where W is the energy consumption [kWh]; Q is the volumetric airflow rate [$m^3\ s^{-1}$]; ΔP is the filter pressure drop [Pa]; t is the operation time [h]; and η_{fan} is the fan efficiency. To account for variability in HVAC system performance, energy consumption was evaluated across three fan efficiency scenarios. An η_{fan} = 0.93 represents the theoretical maximum fan efficiency specified in the manufacturer's manual. An η_{fan} = 0.70 represents a typical value for reasonably new fan installations [68]. Finally, an η_{fan} = 0.50 represents the performance of sub-optimal HVAC systems and is commonly used in previous studies [69,70]. Fan energy consumption was calculated separately for each pre-filter and final-filter installed in each ventilation duct. In this study, results are reported as weekly fan energy consumption [kWh $week^{-1}$], calculated using t = 168 h in Eq. (1) to represent one week of continuous filter operation.

Size-resolved filtration efficiencies were calculated from the merged upstream and downstream number-based PSDs obtained using the SMPS-OPS measurement system. Because upstream and downstream PSDs were collected sequentially rather than simultaneously, efficiency calculations assumed that upstream PSDs remained stable during the short downstream sampling interval. This assumption is justified given the 4-min switching cycle, the 2-min instrument scan time, and the relatively slow variability of outdoor aerosol concentrations on the timescale of individual scans. A similar sampling approach has been utilized and validated in previous studies [57,58,71]. The resulting efficiency data capture the dynamic, long-term evolution of filter performance across $D_{em(o)}$ = 10–10,000 nm.

An in-situ MERV rating was computed following the procedures in ANSI/ASHRAE Standard 52.2–2017. The standard method was slightly modified to accommodate in-situ filter performance evaluation. Instead of using data from the final aging stage, the in-situ MERV rating was determined based on weekly measurements. Consequently, the mean weekly in-situ performance curve, rather than the minimum efficiency curve, was used. Weekly in-situ MERV ratings were derived by aggregating measured size-resolved efficiencies into the three particle size groups defined in Table 12–1 of the Standard [48]: E1 (300–1000 nm), E2 (1000–3000 nm), and E3 (3000–10,000 nm). The resulting weekly E1, E2, and E3 efficiencies were then mapped to the corresponding MERV classification, yielding a time-resolved MERV trajectory for each filter. This in-situ approach provides a quantitative measure of how filtration performance evolves under real outdoor aerosol loading and enables comparison of the long-term aging behavior of mechanical and electret filters, including whether their effective MERV ratings tend to increase, remain stable, or decline over time.

The E1, E2, and E3 values represent the mean filtration efficiencies across all measured particle size bins within each group. Because the SMPS and OPS measurement bins do not align exactly with the standardized boundaries defined in Table 12–1 of the Standard [48], the particle size intervals used for the in-situ MERV calculations differ slightly from those specified in ANSI/ASHRAE Standard 52.2–2017. Table S1 summarizes the instrument-specific size ranges used in the weekly calculations, as well as the corresponding standardized bin definitions. To enable direct comparison with nominal MERV ratings, all size-resolved efficiencies were linearly interpolated to the particle size bins of ANSI/ASHRAE Standard 52.2–2017 prior to assigning the weekly in-situ MERV classification.

3. Results and discussion

This section presents the two-year in-situ aging results obtained from the full-scale HVAC filter test rig. The analysis begins with characterization of the outdoor aerosol particles, including measured in-duct number-based PSDs and the empirical distributions of temperature and RH, which define the environmental conditions under which aging occurred. The stability of the in-duct volumetric airflow rate is then evaluated to confirm near-consistent airflow conditions across all three ventilation ducts throughout the 112-week period. The temporal evolution of filter performance is subsequently examined from three perspectives: (1) resistance to airflow, quantified by changes in filter ΔP, and associated fan energy consumption; (2) in-situ filtration performance, including size-resolved filtration efficiencies from $D_{em(o)}$ = 10–10,000 nm and time-varying in-situ MERV ratings; and (3) filter mass accumulation, assessed through gravimetric measurements of filter mass gain (final mass - initial mass) and analysis of size-resolved contributions to the loaded mass based on SMPS-OPS data. Collectively, these results provide a comprehensive characterization of long-term HVAC filter behavior under continuous exposure to real-world outdoor aerosol.

3.1. Outdoor aerosol size distributions and environmental conditions in the in-situ test rig

The PSD of the outdoor aerosol to which HVAC filters are exposed is a critical determinant of filtration efficiency and the rate of filter loading, acting alongside airflow and filter media characteristics [72,73]. Number-, surface area-, volume-, and mass-based PSDs each emphasize different size fractions relevant to aerosol transport, deposition, and filter loading behavior. Experimental and modeling studies have shown that variations in PSD shape and magnitude strongly influence filter ΔP growth, particle removal efficiency, and DHC [34,36,40,42,43,59,74–76]. Fig. 2 presents the measured number-based PSDs and the corresponding surface area-, volume-, and mass-based PSDs of the outdoor aerosol sampled in the test rig in West Lafayette, IN, U.S., during the first year of aging using the SMPS-OPS system.

The number-based PSD exhibits a pronounced Aitken mode between $D_{em(o)}$ = 10–100 nm, with a peak near $D_{em(o)}$ = 30–40 nm, indicating that most outdoor particles entering the in-situ test rig on a number basis are ultrafine particles. More than 80% of particles fall below $D_{em(o)}$ = 100 nm, underscoring the dominance of sub-100 nm aerosol in real-world outdoor air loading scenarios of HVAC filters. The magnitude of the number PSDs ($dN/dlogD_{em(o)}$ = (2–5) × 10^3 cm^{-3}) and their relatively narrow interquartile ranges reflect stable regional background atmospheric aerosol conditions around West Lafayette, IN, U.S. Both the shape and magnitude of the number-based PSDs are consistent with long-term observations of urban and suburban aerosol in locations across North America and Europe [52]. Downstream of the MERV8 pre-filters, the Aitken mode structure is largely preserved with only modest attenuation in total number concentration, demonstrating that

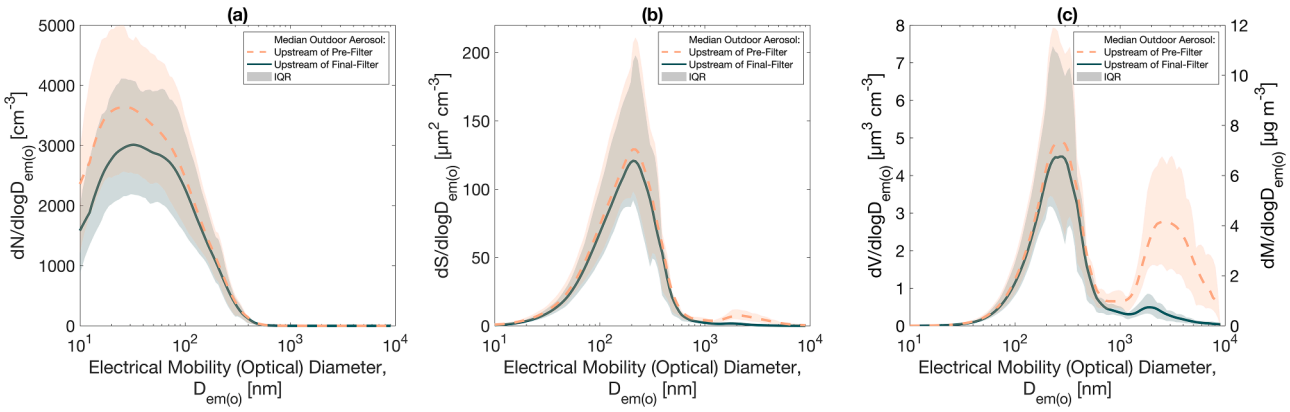

Fig. 2. Median outdoor aerosol particle size distributions (PSDs) measured upstream of the pre- and final-filters during the first year of in-situ aging using the combined SMPS-OPS system from $D_{em(o)}$ = 10–10,000 nm: (a) number-based PSD ($dN/dlogD_{em(o)}$; cm^{-3}); (b) surface area-based PSD ($dS/dlogD_{em(o)}$; $\mu m^2\ cm^{-3}$); and (c) volume-based PSD (left axis; $dV/dlogD_{em(o)}$; $\mu m^3\ cm^{-3}$) and corresponding mass-based PSD (right axis; $dM/dlogD_{em(o)}$; $\mu g\ m^{-3}$), assuming spherical particles with a bulk density of 1.5 g cm^{-3}. Shaded regions indicate the interquartile range (IQR).

pleated pre-filters with efficiencies similar to MERV8 remove only a small fraction of ultrafine particles (see Section 3.3). By contrast, surface area-based PSDs are dominated by accumulation mode particles ($D_{em(o)}$ = 100–400 nm), with nearly identical upstream and downstream shapes across the pre-filters. This indicates that MERV8 pre-filters exert minimal influence on the total outdoor aerosol surface area entering the ventilation duct, with implications for the formation, structure, and spatial distribution of particle deposits within the downstream filter media.

The volume- and mass-based PSDs further highlight the presence of accumulation and coarse mode particles. Upstream of the pre-filter, the mass PSD is distinctly bimodal, with a dominant accumulation mode peak near $D_{em(o)}$ = 200–400 nm and a secondary coarse mode peak extending from 1000–10,000 nm; these are patterns consistent with global compilations of urban mass PSDs [52]. Downstream of the pre-filter, the coarse mode is substantially truncated, confirming the role of MERV8 pre-filters in mitigating coarse particle overloading in the downstream final-filters commonly used in two-stage HVAC filtration systems in commercial buildings. As a result, the final-filters in all three ventilation ducts are exposed predominantly to a sub-micron mass PSD ($dM/dlogD_{em(o)}$ = 4–12 $\mu g\ m^{-3}$) concentrated in the $D_{em(o)}$ = 100–600 nm range. This behavior is directly relevant to ASHRAE Guideline 35, which emphasizes evaluating HVAC filter loading under realistic sub-micron outdoor aerosol conditions, conditions that are not well represented by standardized coarse mode loading dusts. However, during episodic outdoor air pollution events such as wildfires, HVAC filters may encounter markedly different mass PSDs [77–79].

Fig. 3 summarizes the in-duct RH and temperature conditions during the first year of aging. Both the mean and median RH were approximately 64.5%, with RH exceeding 50% for nearly 80% of the loading period, and the filters experienced a broad range of temperatures. Such variability helps explain differences in long-term loading behavior reported across geographic regions, as in-situ filter performance is sensitive to environmental conditions. Elevated RH, often associated with precipitation events, promotes hygroscopic growth of aerosol particles, which can alter both filter pressure drop and removal efficiency [80,81]. For instance, prior studies have shown that hygroscopic particles may reduce filter ΔP at high RH due to restructuring or redistribution of dendritic particle deposits within the filter media, whereas non-hygroscopic particles exhibit little to no RH-dependent effect [35,39,82]. Because outdoor aerosol is a complex mixture containing both hygroscopic and non-hygroscopic components [83–88], the net impact of RH on loading dynamics is difficult to predict a priori. Consequently, the wide range of RH and temperature conditions observed in this study likely contributed to the variability in loading characteristics and underscores the importance of characterizing environmental conditions

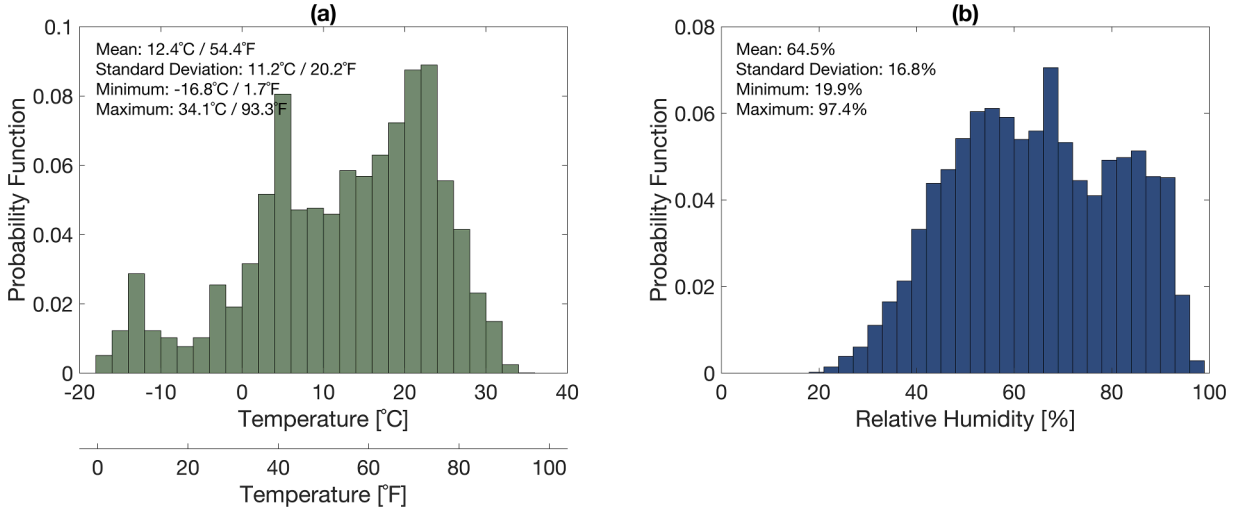

Fig. 3. Probability functions for environmental conditions measured in the test rig during the two-year in-situ aging period: (a) temperature (°C and °F) and (b) relative humidity (RH).

when interpreting long-term in-situ HVAC filter aging behavior.

3.2. Long-term evolution of HVAC filter airflow resistance and fan energy consumption during in-situ aging

Fig. 4 presents the weekly median in-duct volumetric airflow rates, measured filter ΔP, and the corresponding fan energy consumption per filter over the two-year in-situ aging period, with Ducts 1–3 shown from left to right. The first row displays the volumetric airflow rate in each duct. The second row shows the loading curves (ΔP as a function of time) for the MERV8 pre-filters, while the third row presents the loading curves for the final-filters (Duct 1: MERV14, Duct 2: MERV13, and Duct 3: MERV8). The fourth row shows the estimated fan energy consumption associated with the pre-filters, calculated for three fan efficiency scenarios (η_{fan} = 0.93, 0.70, and 0.50), and the fifth row presents the corresponding fan energy consumption for the final-filters. Dashed red lines indicate replacement of the initial MERV8 pre-filters at week 60.

Across all three ventilation ducts, a relatively stable volumetric airflow rate of approximately 2000 $ft^3\ min^{-1}$ was maintained throughout the experiment, supporting comparability of long-term loading behavior among the three filter banks. The largest airflow fluctuations occurred in Duct 3, likely due to its greater distance from the outdoor air intake along the building façade (Fig. 1) and its increased susceptibility to upstream airflow disturbances. The loading curves show exponential

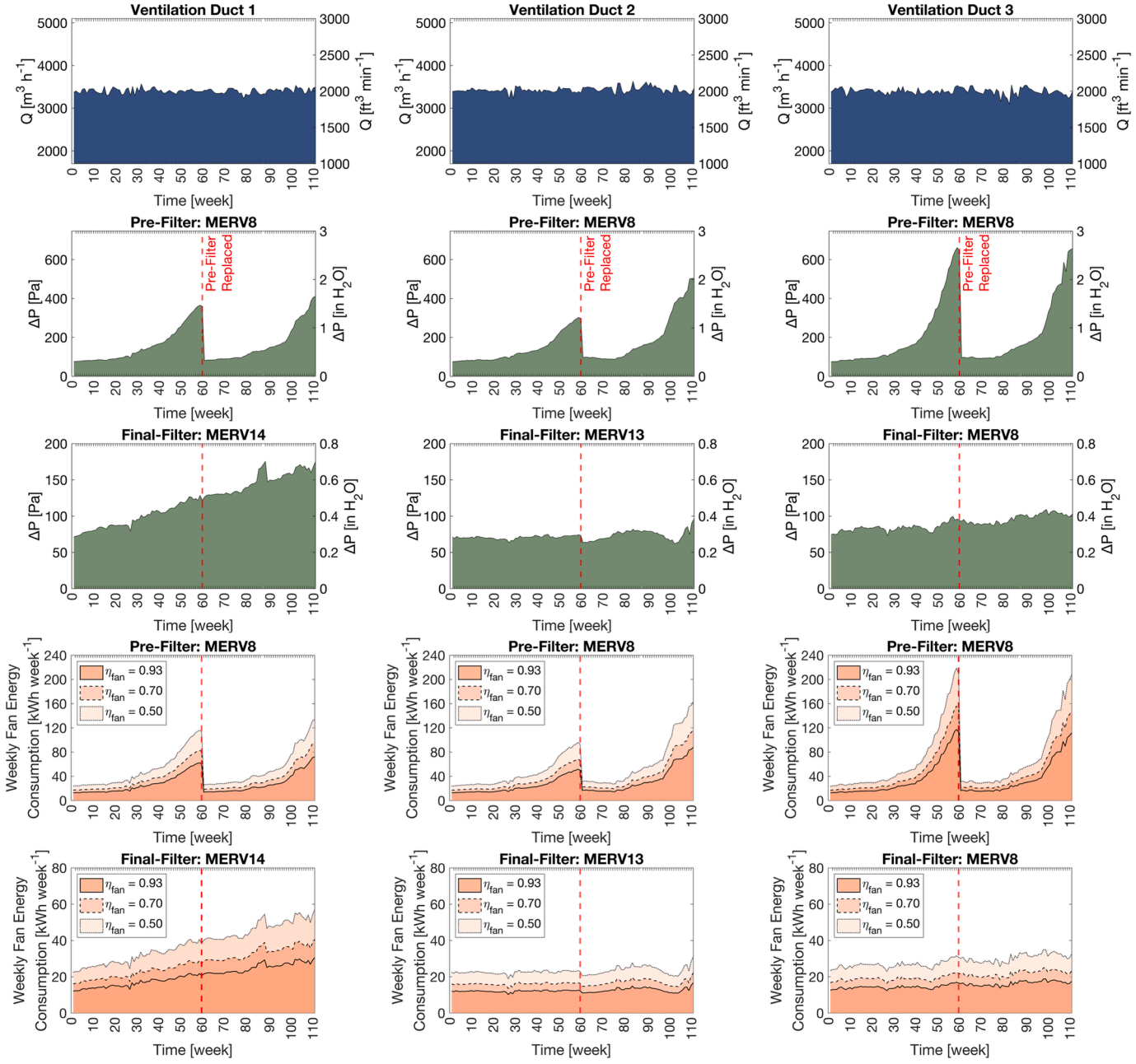

Fig. 4. Weekly median in-duct volumetric airflow rates, measured filter pressure drop (ΔP), and corresponding fan energy consumption per filter over the two-year in-situ aging period, with Ducts 1–3 shown from left to right. The first row shows the volumetric airflow rate in each duct. The second row presents the loading curves (ΔP as a function of time) for the MERV8 pre-filters, and the third row shows the loading curves for the final-filters (Duct 1: MERV14; Duct 2: MERV13; Duct 3: MERV8). The fourth row presents the estimated fan energy consumption associated with the pre-filters, calculated for three fan efficiency scenarios (η_{fan} = 0.93, 0.70, and 0.50), and the fifth row shows the corresponding fan energy consumption for the final-filters. Dashed red lines indicate replacement of the initial MERV8 pre-filters at week 60.

increases in ΔP for the MERV8 pre-filters, consistent with progressive accumulation of sub-micron and coarse mode particles and the corresponding reduction in filter and dust cake porosity. After one year, the pre-filter ΔP exceeded that of the corresponding final-filters by approximately 250–500 Pa. The most pronounced ΔP increase occurred in Duct 3, likely because greater amounts of precipitation entered this duct compared with Ducts 1 and 2. Rain and snow events were occasionally observed to cause minor water leakage into Duct 3, and exposure to excess liquid water may have reduced dust cake porosity and formed thin liquid films on the filter surface, thereby accelerating the increase in filter ΔP [39].

The implications of rising ΔP for HVAC fan energy consumption depend on blower type. Variable-speed (VFD) blowers must draw additional electrical power to maintain constant airflow as ΔP increases, whereas fixed-speed permanent split capacitor (PSC) blowers without speed control experience reduced airflow and correspondingly lower power consumption under higher ΔP [54,55,61,62,89]. Because this study examined speed-controlled operation at a constant volumetric airflow rate, the rising ΔP resulted in substantial increases in weekly fan energy consumption for the MERV8 pre-filters, reaching up to approximately 220 kWh week^{-1} in Duct 3 near the end of each year (Fig. 4). The temporal evolution of weekly fan energy consumption closely mirrors that of filter ΔP, with minor deviations attributable to small fluctuations in volumetric airflow rate. The positive relationship between filter ΔP and fan energy consumption under constant airflow conditions has been documented in previous studies [55,61,68–70,89]. While some investigations, such as Alavy et al. (2020) [61] and Stephens et al. (2010) [89], directly measured fan power draw, others estimated energy consumption based on measured filter ΔP.

Direct comparisons with prior work indicate that the fan energy consumption values estimated in this study are generally lower than those reported for comparable systems. Alavy et al. (2020) [61] examined residential forced-air recirculation systems equipped with electronically commutated motor (ECM) fans and single-stage filtration ranging from MERV8 to MERV14. They reported a three-month energy consumption of approximately 400–600 kWh per filter. In contrast, the three final-filter types evaluated in this study consumed less energy per filter over the same period, based on integration of the weekly energy consumption over three months, ranging from 171.8 to 319.5 kWh for the MERV14 final-filter, 156.6 to 291.3 kWh for the MERV13 final-filter, and 175.2 to 325.9 kWh for the MERV8 final-filter, depending on the assumed fan efficiency (η_{fan} = 0.93–0.50). Similarly, Stephens et al. (2010) [89] monitored residential and light commercial buildings over a one-year period. For a commercial site with an airflow rate comparable to ours (2000 ft^3 min^{-1}), they reported an annual energy consumption of approximately 6988 kWh per filter based on an average fan power draw of ~800 W. By comparison, the one-year integrated energy consumption estimated in the present study ranged from 623.6 kWh (MERV13 final-filter at η_{fan} = 0.93) to 2423.6 kWh (MERV8 pre-filter in Duct 3 at η_{fan}= 0.50) per filter during the first year of operation across the six installed filters.

Consistent with these comparisons, studies that estimate fan energy consumption from filter ΔP measurements also report higher values than those observed here. Considine et al. (2024) [69] monitored a two-stage filtration system for 3000 h and reported a total estimated energy consumption of 2012.5 kWh assuming a fan efficiency of η_{fan} = 0.50. Over an equivalent duration, our filter banks (pre- and final-filters combined) consumed only 869.1 kWh (Duct 2) to 943.7 kWh (Duct 3) at the same assumed fan efficiency. Morgan et al. (2017) [70] evaluated a comparable two-stage filtration system over 1152 h and reported an estimated energy consumption of 652.8 kWh assuming η_{fan} = 0.50, whereas our filter banks consumed between 329.1 kWh (Duct 2) and 350.2 kWh (Duct 3) under the same assumption. Similarly, Montgomery et al. (2012) [68] modeled fan energy consumption of 854 kWh for a MERV8 filter after 4850 h assuming η_{fan} = 0.70, while the present study estimated an integrated energy consumption between 531.6 kWh (MERV8 final-filter in Duct 3) and 596.9 kWh (MERV8 pre-filter in Duct 3) per filter across all MERV8 filters under the same assumed fan efficiency.

While the increasing trend in fan energy consumption aligns with previous studies of speed-controlled fan systems, the absolute values calculated here are consistently lower. These lower values likely reflect several factors affecting filter pressure drop evolution and fan energy estimates. In-situ filter loading depends strongly on upstream aerosol conditions, including number- and mass-based PSDs (shape and magnitude) and aerosol composition, as well as RH variation and restructuring of dendritic particle deposits during aging. In addition, variations in filter media design (material type and mechanical versus electret filtration) and operational airflow rates (e.g., residential versus commercial systems) can significantly influence filter loading behavior and ΔP growth rates. Differences in system configuration and variable fractions of outdoor versus recirculated indoor air may further affect the in-situ aging conditions experienced by the filters. Additional uncertainty arises from the fan efficiencies assumed in the energy calculations. As noted in EUROVENT 4/21–2019 [67], actual fan efficiency can vary substantially depending on fan design, operating speed, and system layout, and in some cases may be as low as η_{fan} = 0.25. Finally, studies that directly measure fan power typically account for the total system pressure drop, including heat exchangers and ductwork, whereas the present analysis isolates the energy penalty associated solely with filter pressure drop.

After week 60, the replacement MERV8 pre-filters exhibited loading trajectories nearly identical to those of the original filters, confirming the repeatability of the in-situ aging process between the first and second years. Although prior laboratory studies often report slower ΔP growth when the challenge aerosol contains a higher fraction of coarse particles due to the formation of a more permeable surface dust cake [34,36,43,76], those studies typically maintain a constant total particle concentration across different size fractions. In the present experiment, the more pronounced ΔP increase observed for the MERV8 pre-filter relative to the downstream MERV8 final-filter in Duct 3 is attributable to the higher outdoor aerosol concentrations encountered upstream of the pre-filter (Fig. 2). Unlike the final-filters, the pre-filters were exposed to elevated concentrations of both sub-micron and coarse mode particles, resulting in greater overall particle loading and, consequently, a larger increase in ΔP (Fig. 2). Thus, differences in total particle number and mass loading, rather than dust cake structure alone, explain the observed ΔP behavior.

Among the final-filters, the MERV14 exhibited the largest increases in ΔP and weekly fan energy consumption over two years of loading, with approximate increases of 100 Pa and 20 kWh week^{-1}. A sharp decrease in ΔP near week 90 was later traced to minor physical damage to the filter media discovered upon removal from the rig, although the exact cause remains uncertain. The MERV13 final-filter maintained a comparatively stable ΔP throughout the aging period, reflecting both its larger media area relative to the MERV8 final-filter and the reduction in particle loading associated with electret charge decay, as discussed in Section 3.3. Similar temporal trends for electret bag filters have been reported previously [69]. Despite their higher initial efficiencies, the MERV13 and MERV14 final-filters contributed far less to the total airflow resistance and energy penalty of the two-stage filter bank than the more heavily loaded MERV8 pre-filters. Although the MERV14 final-filter maintained substantially higher particle removal efficiency than the MERV8 final-filter (Section 3.3), its ΔP after two years was only approximately 60 Pa greater. These findings indicate that the pre-filter, operated for approximately one year of continuous outdoor aerosol exposure before replacement after the first year of the experiment, overwhelmingly governs long-term airflow resistance and fan energy consumption under the extended service interval considered here. In practice, shorter pre-filter replacement intervals could reduce the associated pressure drop and fan energy penalties in variable-speed blower

systems. At the same time, appropriate use of pre-filtration extends the service life and stabilizes the performance of higher-efficiency downstream filters in real HVAC systems.

3.3. Long-term evolution of size-resolved filtration efficiency during in-situ aging

The size-resolved filtration efficiency dataset for each test duct was divided into two distinct operational periods corresponding to the scheduled replacement of the MERV8 pre-filters: (a) Year 1, spanning weeks 1–60, during which all pre-filters were the original installed units; and (b) Year 2, spanning weeks 61–112, following installation of new pre-filters at week 60. In Figs. 5–7, weekly progression is represented by color gradients from blue to pink for both periods, illustrating aging from weeks 1–60 (Year 1) and weeks 61–112 (Year 2). For clarity, only mean filtration efficiency curves are shown. Given the high-resolution of the combined SMPS and OPS measurements (119 particle size bins), measurement variability is presented in Figures S2-S4 as mean ± standard deviation for six representative time points (initial, midpoint, and endpoint of each year).

Due to the sequential sampling strategy, wherein a single SMPS-OPS instrument suite rotated weekly among the three ventilation ducts, a one-week temporal offset exists between the initial and final sampling points for each duct. Nevertheless, this systematic staggering does not affect the comparability of long-term trends within or across ducts, as each filter section was sampled on a consistent weekly cycle throughout the full 112-week period. Size-resolved efficiency data below $D_{em(o)}$ = 300 nm are unavailable during the final six weeks due to SMPS downtime caused by a hardware malfunction requiring manufacturer maintenance. During this period, the OPS remained operational, allowing continued measurements for particles with $D_{em(o)} \geq 300$ nm. Despite this limitation, the overall trend analysis remains robust given the extensive dataset collected prior to the outage.

3.3.1. Size-resolved filtration efficiency evolution in Duct 1 (MERV8 pre-filter and MERV14 final-filter)

Fig. 5 presents the mean size-resolved filtration efficiency curves for Duct 1 from $D_{em(o)}$ = 10–10,000 nm, constructed by linearly interpolating across particle size bins measured by the SMPS and OPS. The color gradients from blue to pink denote the weekly progression of aging from weeks 3–60 (Year 1) and weeks 63–111 (Year 2), illustrating the temporal evolution of filtration performance.

Consistent with filtration theory and prior in-situ studies [57,73,90,91], the most penetrating particle size (MPPS) for both the MERV8 pre-filter and the MERV14 final-filter occurred between $D_{em(o)}$ = 100 and 500 nm, with the highest efficiencies observed for the largest, and in some cases the smallest, particle sizes measured. These results reinforce the need to extend standardized MERV evaluations below 300 nm, as the MPPS of many filter types falls at or below this threshold. As expected, based on its higher media efficiency, the MERV14 final-filter removed ultrafine particles far more effectively than the MERV8 pre-filter, consistent with prior experimental observation [58,60–62]. In addition, the MERV8 pre-filters tested in this duct displayed nearly identical initial size-resolved efficiencies across Years 1 and 2, demonstrating the reproducibility of mechanical filter performance during long-term aging.

The slight decline in filtration efficiency below $D_{em(o)}$ = 20 nm for the MERV14 final-filter, observed intermittently during select weeks of Year 1, aligns with multiple in-situ studies that have documented comparable drop-offs in the $D_{em(o)}$ = 10–20 nm size regime [57–59,71]. Across these studies, absolute efficiency reductions for sub-20 nm particles typically range from 5% to 15%, consistent with the ~10–20% decline observed here. For example, Stephens et al. (2013) [57] reported a localized ~5% efficiency reduction (from ~20% at $D_{em(o)}$ = 15 nm to

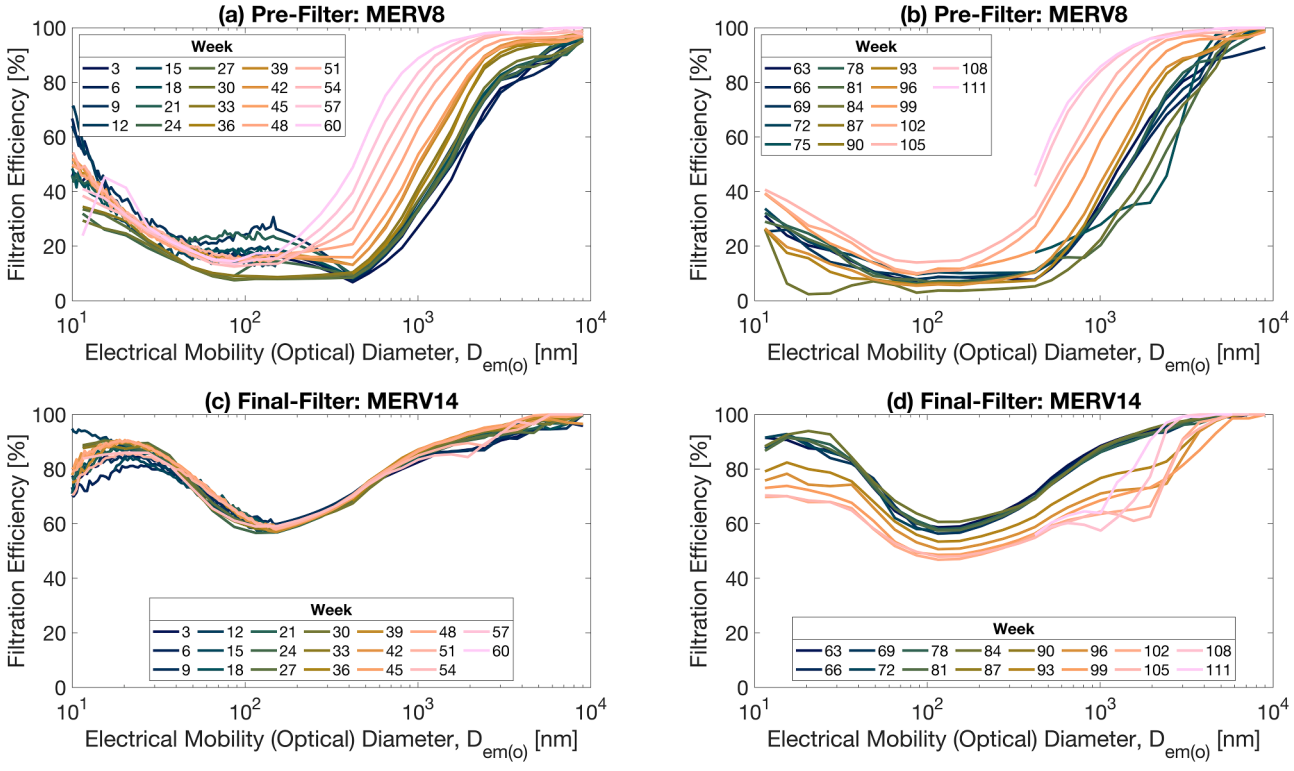

Fig. 5. In-situ size-resolved filtration efficiencies for Duct 1 from $D_{em(o)}$ = 10–10,000 nm during (a, c) Year 1 and (b, d) Year 2 of outdoor aerosol aging. Weekly progression is indicated by color gradients from blue to pink, representing aging from weeks 3–60 (Year 1) and weeks 63–111 (Year 2). Panels (a) and (b) show weekly filtration efficiency curves for the MERV8 pre-filter (replaced after Year 1), while panels (c) and (d) show the corresponding curves for the MERV14 final-filter. Efficiency curves were constructed by linearly interpolating across particle size bins measured by the combined SMPS-OPS system.

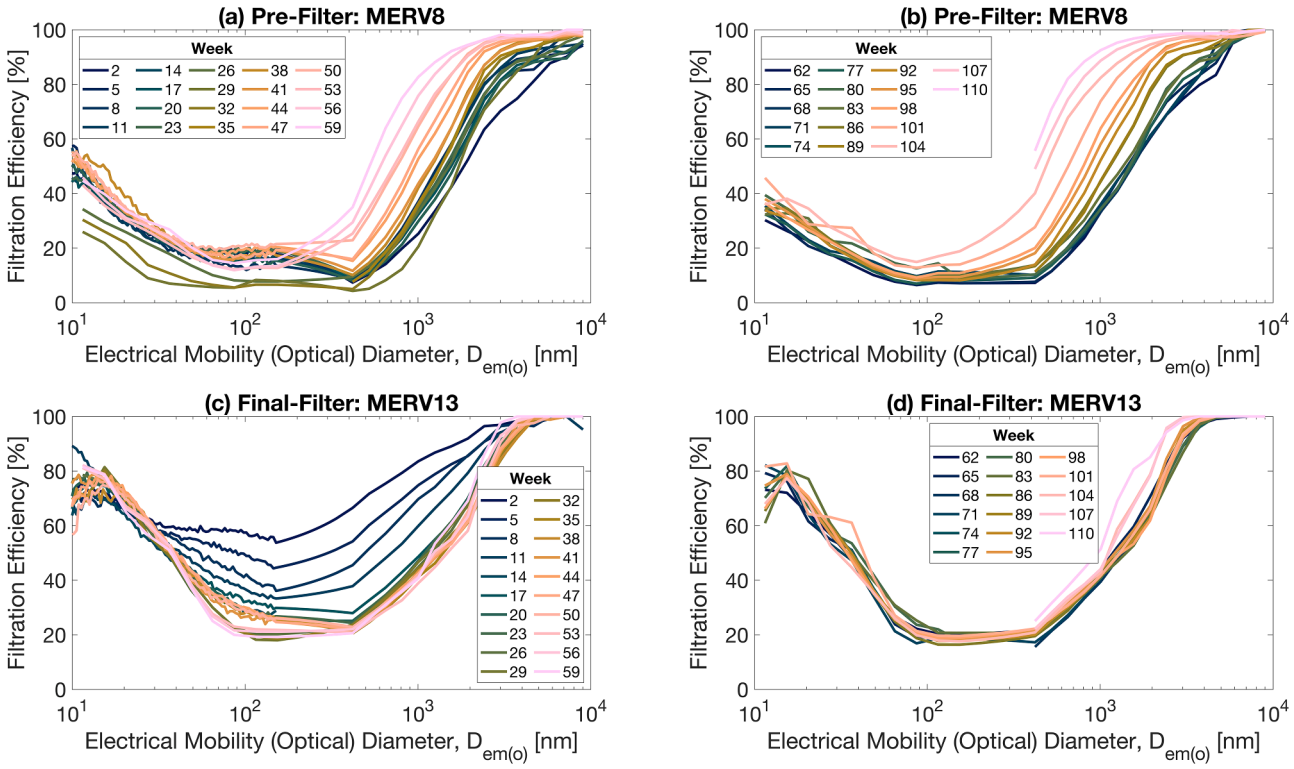

Fig. 6. In-situ size-resolved filtration efficiencies for Duct 2 from $D_{em(o)}$ = 10–10,000 nm during (a, c) Year 1 and (b, d) Year 2 of outdoor aerosol aging. Weekly progression is indicated by color gradients from blue to pink, representing aging from weeks 2–59 (Year 1) and weeks 62–110 (Year 2). Panels (a) and (b) show weekly filtration efficiency curves for the MERV8 pre-filter (replaced after Year 1), while panels (c) and (d) show the corresponding curves for the MERV13 final-filter. Efficiency curves were constructed by linearly interpolating across particle size bins measured by the combined SMPS-OPS system.

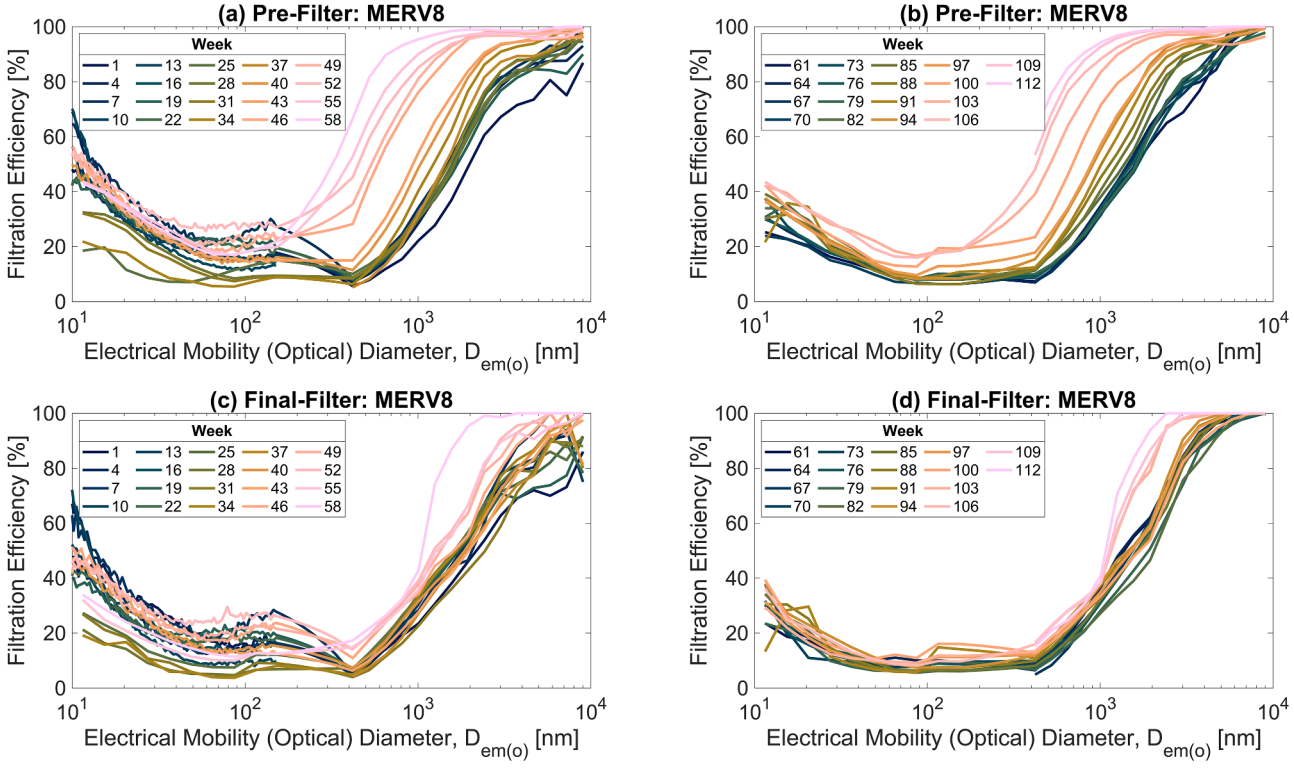

Fig. 7. In-situ size-resolved filtration efficiencies for Duct 3 from $D_{em(o)}$ = 10–10,000 nm during (a, c) Year 1 and (b, d) Year 2 of outdoor aerosol aging. Weekly progression is indicated by color gradients from blue to pink, representing aging from weeks 1–58 (Year 1) and weeks 61–112 (Year 2). Panels (a) and (b) show weekly filtration efficiency curves for the MERV8 pre-filter (replaced after Year 1), while panels (c) and (d) show the corresponding curves for the MERV8 final-filter. Efficiency curves were constructed by linearly interpolating across particle size bins measured by the combined SMPS-OPS system.

~15% at $D_{em(o)}$ = 8 nm) for an electrostatically charged MERV11 filter. Fazli et al. (2019) [58] evaluated 50 commercial HVAC filters and observed similar reductions across multiple filter classes, ranging from ~5% for a MERV8 filter to as much as 15% for MERV4 and MERV13 filters below $D_{em(o)}$ = 20 nm. Likewise, Li et al. (2019) [59] reported a ~10% decrease in efficiency for a MERV11 electret filter as particle size decreased from $D_{em(o)}$ = 30 nm to 10 nm. This characteristic reduction also extends beyond HVAC filtration; Zhao et al. (2017) [71] observed a comparable ~10% increase in penetration (i.e., decrease in efficiency) for building envelope transport between $D_{em(o)}$ = 20 nm and 10 nm. Collectively, these prior field measurements provide empirical support for the magnitude of the sub-20 nm efficiency reduction observed in this study.

While prior in-situ filtration studies have not provided a definitive explanation for this phenomenon, several plausible mechanisms have been proposed: (1) formation of new sub-20 nm particles via outdoor ozone reactions with filter-deposited material, generating low-volatility compounds that nucleate and grow, thereby elevating downstream number concentrations and reducing in-situ efficiency [30,92–100]; (2) particle detachment from the filter or dust cake under aerodynamic shear or structural destabilization, increasing downstream particle number concentrations [101,102]; (3) potential size-dependent limitations of electrostatic interactions in the nanoscale regime, likely minor for non-electret filters (e.g., the MERV14 final-filter) and possibly reflecting residual charges carried by outdoor aerosol particles [103]; and (4) measurement artifacts associated with SMPS transfer functions and diffusional broadening, which can amplify counting uncertainties for sub-20 nm particles [104–106]. These mechanisms are not mutually exclusive, and resolving their relative contributions would require targeted experimental investigation.

Throughout the first year of operation, the MERV14 final-filter exhibited remarkably stable size-resolved filtration efficiency across the full measured range from $D_{em(o)}$ = 10–10,000 nm. As a non-electrostatic V-cell filter with a large media area, its performance remained essentially unchanged despite sustained outdoor aerosol loading. The MERV14 consistently maintained greater than 55% removal efficiency for particles within the $D_{em(o)}$ = 100–500 nm size range, near the MPPS, even after nearly 90 weeks of continuous operation. Similarly, filtration efficiency exceeded 70% for the smallest measured ultrafine particles ($D_{em(o)}$ = 10–50 nm) over this same period. This stability demonstrates the robustness of mechanical (non-electret) filter media in removing outdoor aerosol particles during long-duration HVAC applications. A sharp decline in filtration efficiency was observed after approximately week 90, coinciding with a sudden reduction in pressure drop (Fig. 4). Follow-up inspection revealed minor physical damage to the filter media. As shown in Figure S5, the mini-pleated filter media detached from the central vertical support frame. This detachment allowed the pleated pack to arch significantly under velocity pressure, forming a rectangular gap, while the filtration media itself remained largely intact. Although the cause could not be determined, the magnitude of the resulting efficiency loss, approximately 15–25% across the measured size range, provides a useful real-world illustration of how incidental mechanical degradation can affect HVAC filter performance in practice.

3.3.2. Size-resolved filtration efficiency evolution in Duct 2 (MERV8 pre-filter and MERV13 final-filter)

Fig. 6 presents the weekly mean size-resolved filtration efficiency curves for Duct 2. In contrast to the stable performance of the mechanical MERV14 filter in Duct 1, the MERV13 electret final-filter in Duct 2 exhibited a gradual decline in efficiency across much of the measured size range over the two-year aging period. Notably, opposing temporal trends were observed within the same duct: the MERV8 mechanical pre-filter showed increasing efficiency with loading, whereas the MERV13 electret final-filter showed decreasing efficiency. After two years, the MERV8 pre-filter achieved a higher efficiency (20–30%) than the MERV13 final-filter (~20%) near the MPPS range ($D_{em(o)}$ = 100 to 500 nm), underscoring the divergent aging behaviors of mechanical versus electret filter media during outdoor aerosol aging.

The performance degradation of the MERV13 electret filter is consistent with established mechanisms governing electret aging. Electret filtration efficiency is the sum of mechanical and electrostatic collection mechanisms, and numerous studies have shown that loss of electrostatic charge generally outpaces any gains in mechanical efficiency during particle loading. Charge decay is further accelerated by aerosol neutralization and moisture exposure, both of which suppress Coulombic and dielectrophoretic particle capture [39,41,45,59,107–112]. In this study, the filters were exposed to sustained elevated humidity (mean RH = 64.5%, with maxima exceeding 90%; Fig. 3), conditions known to promote rapid electret charge dissipation. Consequently, the decline in filtration efficiency is accompanied by a suppressed increase in ΔP over time (Fig. 4), a characteristic hallmark of electret media aging.

These observations align with previous research: Liu et al. (2020) reported substantial loss of surface potential and efficiency after only one hour at 90% RH [45], and Lee et al. (2020) documented measurable charge decay within minutes under similar conditions [110]. Additional studies have demonstrated that particle loading itself reduces the initial electrostatic effect in electret fibers [79,113]. Elevated RH also increases dust cake porosity, further limiting ΔP growth [114]. Collectively, the results from Duct 2 highlight the pronounced sensitivity of MERV13 electret filters to humid, aerosol-rich outdoor air and illustrate the contrasting long-term behavior of electret versus mechanical filters under real-world aging conditions.

Furthermore, filters operating in real-world HVAC systems are exposed to complex mixtures of elemental carbon (soot) and organic carbon from both episodic air pollution events, such as wildfires and agricultural burning, and routine residential sources, such as wood combustion (e.g., fireplaces and wood-burning stoves). These carbonaceous aerosols may further accelerate electret charge decay, compounding the effects of RH and particle loading observed for the MERV13 final-filter. In particular, soot-rich particles can promote more rapid charge neutralization than inorganic or semi-volatile organic aerosol components typically associated with mechanical loading. As conductive soot particles accumulate on the filter media, they may facilitate charge dissipation, weakening Coulombic and dielectrophoretic particle capture and contributing to the observed decline in filtration efficiency over time. Consequently, exposure to soot-rich outdoor aerosols may further degrade MERV13 electret filter performance and shorten their effective service life, accelerating the transition toward lower, purely mechanical filtration efficiency [79,109].

3.3.3. Size-resolved filtration efficiency evolution in Duct 3 (MERV8 pre-filter and MERV8 final-filter)

Fig. 7 presents the weekly mean size-resolved filtration efficiency curves for Duct 3. Both the MERV8 pre-filter and MERV8 final-filter exhibit a pronounced increase in efficiency for particles larger than $D_{em(o)}$ = 300 nm over the two-year aging period, with the pre-filter showing the greater enhancement. In contrast, filtration efficiencies for particles smaller than $D_{em(o)}$ = 300 nm remain comparatively stable throughout aging for both filters. Minor discrepancies in the sub-300 nm size range, most notable between weeks 25 and 35, are likely attributable to alternating use of two SMPS instruments [64,71,115].

The more substantial increase in filtration efficiency observed for the MERV8 pre-filter relative to the MERV8 final-filter in Duct 3 reflects its exposure to higher upstream outdoor aerosol concentrations. As shown by the number- and mass-based PSDs in Fig. 2, the pre-filter encounters elevated levels of both sub-micron and coarse mode particles, promoting faster and denser formation of dendritic particle structures within the filter media. This accelerated development of the outdoor aerosol particle deposits leads to a sharper rise in ΔP (Fig. 4) and a correspondingly greater enhancement in mechanical filtration efficiency. These results

reinforce the central role of particle-layer accumulation in shaping the performance evolution of mechanical filter media during long-term HVAC filter aging processes.

The Duct 3 results show that MERV8 filters provide minimal removal of Aitken and accumulation mode outdoor aerosol particles between $D_{em(o)}$ = 30–300 nm, with both the pre- and final-filters maintaining efficiencies of only 5–30% throughout the aging period. This limitation is significant because the current MERV rating system evaluates filtration efficiency only for particles larger than 300 nm, offering limited insight into filter behavior for the sub-300 nm size fractions that dominate outdoor aerosol populations on both a number and surface area basis [52]. These particles are especially important because many major outdoor air pollution sources generate large quantities of sub-300 nm aerosol, including wildfires, industrial activities, tailpipe and non-tailpipe traffic emissions, atmospheric new particle formation events, and sea spray aerosol [77–79,116–119]. As shown in Fig. 2, outdoor aerosol number- and surface area-based PSDs are dominated by sub-300 nm particles, which also exhibit high deposition fractions throughout the human respiratory system. Evaluating the transport and removal of these particles in commercial HVAC systems with substantial outdoor air intake is therefore essential for predicting occupant exposure to aerosol particles of outdoor origin [23–26].

3.4. *In-situ MERV rating evolution during two years of outdoor aerosol aging*

The in-situ MERV rating was evaluated on a weekly basis to track how each filter's effective standardized performance evolved under real-world outdoor aerosol loading. Following ANSI/ASHRAE Standard 52.2–2017, weekly size-resolved filtration efficiencies were aggregated into the three required particle size groups: E1 (300–1000 nm), E2 (1000–3000 nm), and E3 (3000–10,000 nm). The resulting efficiencies were then mapped to the corresponding MERV classifications [48], as described in Section 2.5.

Fig. 8 shows the temporal evolution of the in-situ MERV ratings for Duct 1, with red dashed lines indicating the pre-filter replacement at week 60. Periodic gaps in the bar charts reflect unavoidable instrumentation interruptions during the two-year aging period, primarily due to OPS pump malfunctions. Despite these intervals, the dataset is sufficient to resolve long-term trends. The initial recorded MERV rating for the MERV8 pre-filter was MERV10, attributable to the three-week delay before the first measurement resulting from the rotating SMPS-OPS sampling schedule. The pre-filter's in-situ MERV rating increased steadily from MERV10 to MERV13 over the first year of aging. After installation of a new pre-filter, the MERV rating again began at MERV10 and rose over time following a nearly identical trajectory. Among the three efficiency groups, the largest increases occurred in E2 (1000–3000 nm), which rose from approximately 50% to 90% over 60 weeks. E3 (3000–10,000 nm) increased more modestly, from approximately 87% to 98%. These patterns confirm that mechanical pleated MERV8 filters become increasingly effective at removing coarse and accumulation mode particles from $D_{em(o)}$ = 300–10,000 nm, which dominate the outdoor aerosol mass PSDs (Fig. 2), during prolonged aging. For the MERV14 final-filter, no substantial change in MERV rating or in the E1-

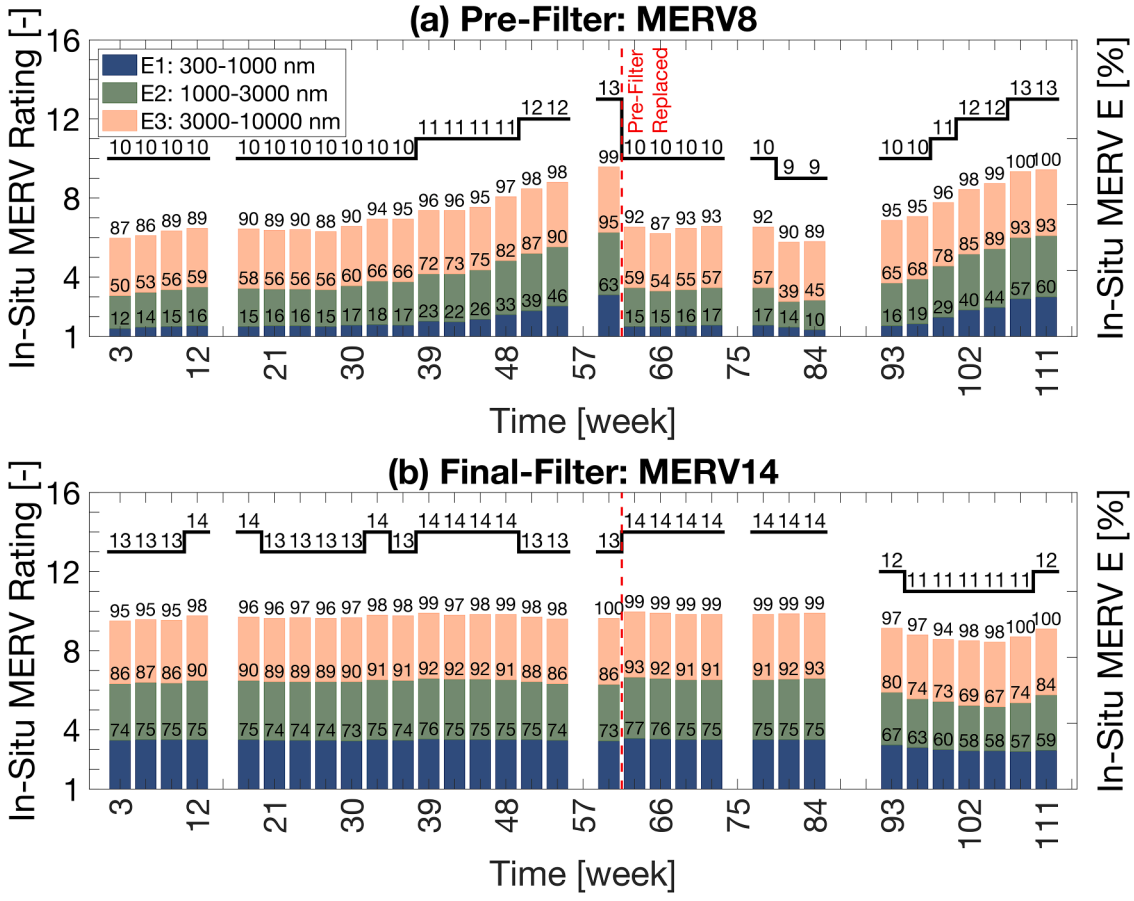

Fig. 8. Weekly in-situ MERV ratings and corresponding efficiency groups (E1, E2, and E3) for filters in Duct 1 during the two-year outdoor aerosol aging period. Panel (a) shows the MERV8 pre-filter, and panel (b) shows the MERV14 final-filter. In each panel, the black line denotes the weekly in-situ MERV rating (left axis), and the stacked bars represent the aggregated E1 (300–1000 nm; blue), E2 (1000–3000 nm; green), and E3 (3000–10,000 nm; dark pink) efficiencies (right axis) used to assign the weekly MERV classification following ANSI/ASHRAE Standard 52.2–2017. Dashed red vertical lines indicate replacement of the MERV8 pre-filter at week 60.

E3 categories was observed prior to the minor filter media damage event at week 90. The in-situ rating oscillated between MERV13 and MERV14, driven mainly by small week-to-week variations in E2 efficiency.

Fig. 9 illustrates the temporal evolution of the in-situ MERV ratings for the filters installed in Duct 2. The MERV8 pre-filter again showed a substantial increase in performance, rising to an in-situ MERV13 after 60 weeks of aging. This surpassed the MERV13 final-filter, whose rating declined to MERV10 over the same period. The replacement pre-filter exhibited a nearly identical upward trajectory during Year 2. In contrast, the in-situ MERV rating for the MERV13 electret final-filter decreased from MERV12 to MERV10 before partially recovering and stabilizing at approximately MERV11. This pattern may be linked to dust cake development on the filter media during extended aging. The observed decline aligns with the size-resolved efficiency trends in Fig. 6 and is consistent with electret aging mechanisms, wherein the loss of electrostatic charge, accelerated by outdoor aerosol deposition and humidity exposure, reduces E1-E3 efficiencies over time. Among the three efficiency groups, the largest reductions occurred in E1 (300–1000 nm), underscoring that electret media are particularly susceptible to performance degradation in this size range. These results demonstrate that different filter types can exhibit divergent in-situ aging behaviors, with mechanical MERV8 filters increasing in apparent MERV rating over time while electret MERV13 media experience a gradual decline.

Fig. 10 illustrates the temporal evolution of the in-situ MERV ratings and associated efficiency categories for both the MERV8 pre-filter and final-filter installed in Duct 3. For the MERV8 pre-filter, the in-situ MERV rating increased steadily, reaching MERV14 just prior to replacement at week 60. The replacement pre-filter followed a nearly identical trajectory, again rising to approximately MERV13 by the end of the second year. The MERV8 final-filter also showed performance gains, increasing from an initial in-situ MERV rating of 8–9 to roughly MERV11 after two years of aging. Correspondingly, the E1-E3 efficiency profiles for the MERV8 final-filter exhibit incremental improvements across all size categories. The parallel trends observed for both pre- and final MERV8 filters indicate that aging under real-world outdoor aerosol conditions can substantially enhance the apparent MERV rating of pleated mechanical filters, with the largest gains occurring for particles in the 1000–10,000 nm range.

Taken together, the in-situ MERV results underscore the importance of accounting for temporal changes in filtration efficiency when evaluating mitigation strategies for outdoor aerosol particles in buildings, particularly within the sub-micron size range. Although the present study focuses on outdoor aerosol aging, these trends are also relevant for indoor-generated aerosol particles, including airborne pathogens such as SARS-CoV-2, which has been detected in particles spanning approximately 250–10,000 nm, with elevated concentrations observed between 250 and 1000 nm [120,121]. Because particles in this size range fall largely within the E1 category (300–1000 nm), changes in E1 efficiency are particularly consequential for virus-relevant aerosol removal in commercial buildings. For example, in Duct 2, the MERV8 pre-filter's E1 efficiency, which is especially relevant for SARS-CoV-2 mitigation, increased substantially during aging, rising from 12% to 51% over the first year. In contrast, the MERV13 electret final-filter exhibited a pronounced decline in E1 efficiency, decreasing from 72% to 27% over the

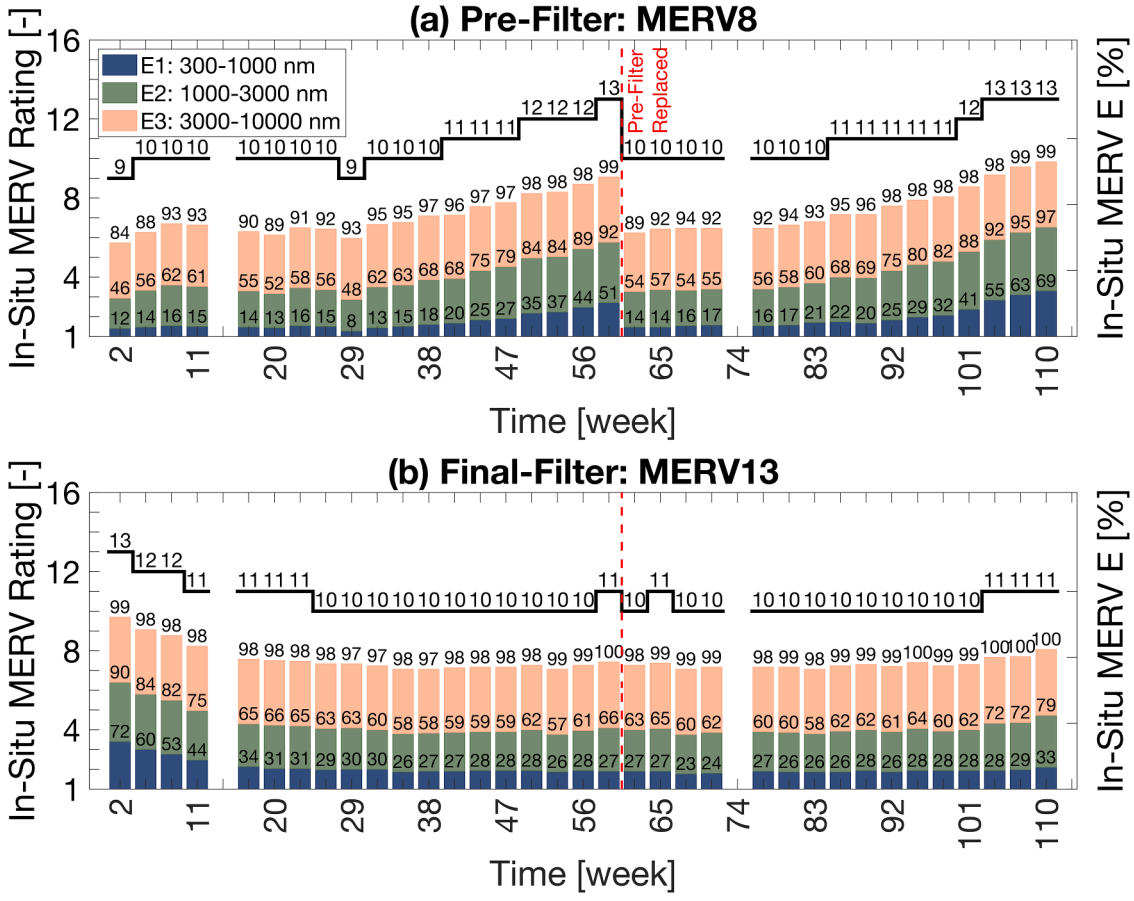

Fig. 9. Weekly in-situ MERV ratings and corresponding efficiency groups (E1, E2, and E3) for filters in Duct 2 during the two-year outdoor aerosol aging period. Panel (a) shows the MERV8 pre-filter, and panel (b) shows the MERV13 final-filter. In each panel, the black line denotes the weekly in-situ MERV rating (left axis), and the stacked bars represent the aggregated E1 (300–1000 nm; blue), E2 (1000–3000 nm; green), and E3 (3000–10,000 nm; dark pink) efficiencies (right axis) used to assign the weekly MERV classification following ANSI/ASHRAE Standard 52.2–2017. Dashed red vertical lines indicate replacement of the MERV 8 pre-filter at week 60.

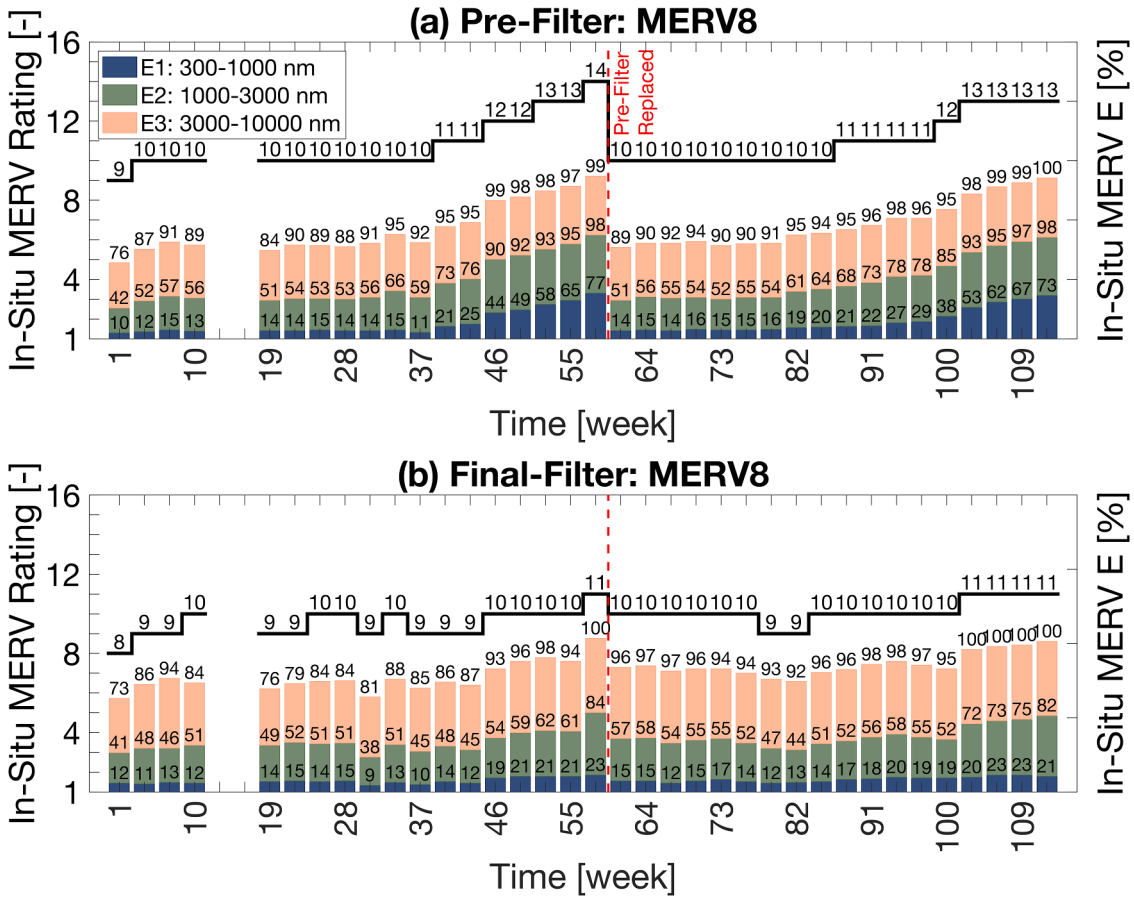

Fig. 10. Weekly in-situ MERV ratings and corresponding efficiency groups (E1, E2, and E3) for filters in Duct 3 during the two-year outdoor aerosol aging period. Panel (a) shows the MERV8 pre-filter, and panel (b) shows the MERV8 final-filter. In each panel, the black line denotes the weekly in-situ MERV rating (left axis), and the stacked bars represent the aggregated E1 (300–1000 nm; blue), E2 (1000–3000 nm; green), and E3 (3000–10,000 nm; dark pink) efficiencies (right axis) used to assign the weekly MERV classification following ANSI/ASHRAE Standard 52.2–2017. Dashed red vertical lines indicate replacement of the MERV 8 pre-filter at week 60.

same period. These divergent behaviors highlight how different filter media evolve under real-world aging conditions and reinforce the need to consider temporal efficiency shifts, rather than relying solely on initial, laboratory-rated MERV values, when designing filtration-based exposure-reduction strategies for both outdoor- and indoor-derived particles, including respiratory viruses.

However, given that the pressure drop increased by more than 200 Pa, the gain in E1 efficiency for the MERV8 pre-filter in Duct 2 is insufficient to justify the associated energy penalty (Fig. 4). It is likely more effective to employ intrinsically higher-efficiency filter media (e.g., MERV14) rather than relying on secondary gains from in-situ particle loading to enhance filtration performance. Moreover, the observed increase in E1 efficiency was non-linear and delayed, becoming substantial only after approximately 40 weeks of operation. Consequently, the system operated at relatively low E1 efficiency for much of the service period. Collectively, these findings suggest that the energy costs associated with increased pressure drop may outweigh the filtration benefits. As a result, dual-MERV8 configurations may offer limited practical advantage in HVAC applications. Because the secondary MERV8 final-filter provides only modest improvement in sub-100 nm ultrafine particle removal, this configuration may offer limited additional benefit for outdoor ultrafine particle control, as a single-stage MERV8 system would yield comparable performance in this size range with lower energy consumption.

3.5. *Size-resolved mass loading in final-filters during in-situ aging*

Table 3 summarizes the mass gain of the final-filters after two years

Table 3
Gravimetric and SMPS-OPS estimated filter mass gain for final-filters during the two-year outdoor aerosol aging period.

In-Situ Aging Duration: 2 Years		MERV14 Final-Filter	MERV13 Final-Filter	MERV8 Final-Filter
Initial Filter Mass [g]		5526.16	2523.38	517.44
Final Filter Mass [g]		5791.80	2687.80	619.60
Gravimetric ΔFilter Mass [g]		256.64	164.42	102.16
SMPS-OPS Estimated ΔFilter Mass [g]	$\rho = 1.50$ [g cm^{-3}]	159.40	75.80	37.30
	$\rho = 1.25$ [g cm^{-3}]	132.90	63.30	31.10
	$\rho = 1.00$ [g cm^{-3}]	106.30	50.60	24.90

of outdoor aerosol aging in the in-situ test rig. Higher-rated filters exhibited greater mass accumulation, consistent with their higher intrinsic filtration efficiencies. The initial masses of the MERV14, MERV13, and MERV8 final-filters were 5526.16 g, 2523.38 g, and 517.44 g, respectively. After the aging period, the final masses increased to 5791.80 g, 2687.80 g, and 619.60 g, corresponding to net mass gains (ΔFilter Mass) of 256.64 g, 164.42 g, and 102.16 g, respectively. The largest mass gain occurred in the MERV14 final-filter, reflecting its enhanced ability to capture and retain outdoor aerosol particles under real-world operating conditions. Although minor media damage occurred in the MERV14 final-filter at week 90, potentially allowing some captured particles to be lost, it still exhibited the greatest overall mass increase.

It is important to note that the mass gains reported here do not represent the absolute DHC of the filters. Instead, they reflect the mass accumulated at the conclusion of the two-year in-situ loading period, rather than at the point when each filter reached its end-of-life ΔP limit. Because the final-filters had not yet reached their maximum allowable ΔP, the observed mass gains capture only a portion of each filter's potential DHC. For example, the MERV13 final-filter exhibited a considerably lower final ΔP than the MERV14 and MERV8 final-filters, implying a longer remaining service life and a correspondingly larger unutilized DHC. Thus, direct comparisons of absolute mass gain across filters should be interpreted with caution. Even so, the measured mass gains provide useful insight into the relative particle capture performance of each filter type over a standardized, multi-year period of outdoor aerosol loading.

The calculated final-filter mass gain based on SMPS-OPS measurements significantly underestimates the gravimetric measurements by 63.7%, 53.1%, and 37.5% for the MERV8, MERV13, and MERV14 final-filters, respectively (Figure S6). This discrepancy can be attributed to several factors, including uncertainty in assumed outdoor aerosol particle density and the under-sampling of super-10 μm particles, which can contribute substantially to total mass. In addition, the gravimetric mass includes contributions from condensed low-volatility organic and inorganic species [122,123], water uptake [87,88], microbial growth [124], and ozone-initiated formation of secondary species on the filter media [125], none of which are captured by SMPS-OPS measurements. For example, Bi et al. (2018) [122] and Wan et al. (2022) [123] reported elevated concentrations of low-volatility organic species, including phthalates, organophosphates, and polycyclic aromatic hydrocarbons, in accumulated HVAC filter dust. These findings suggest that

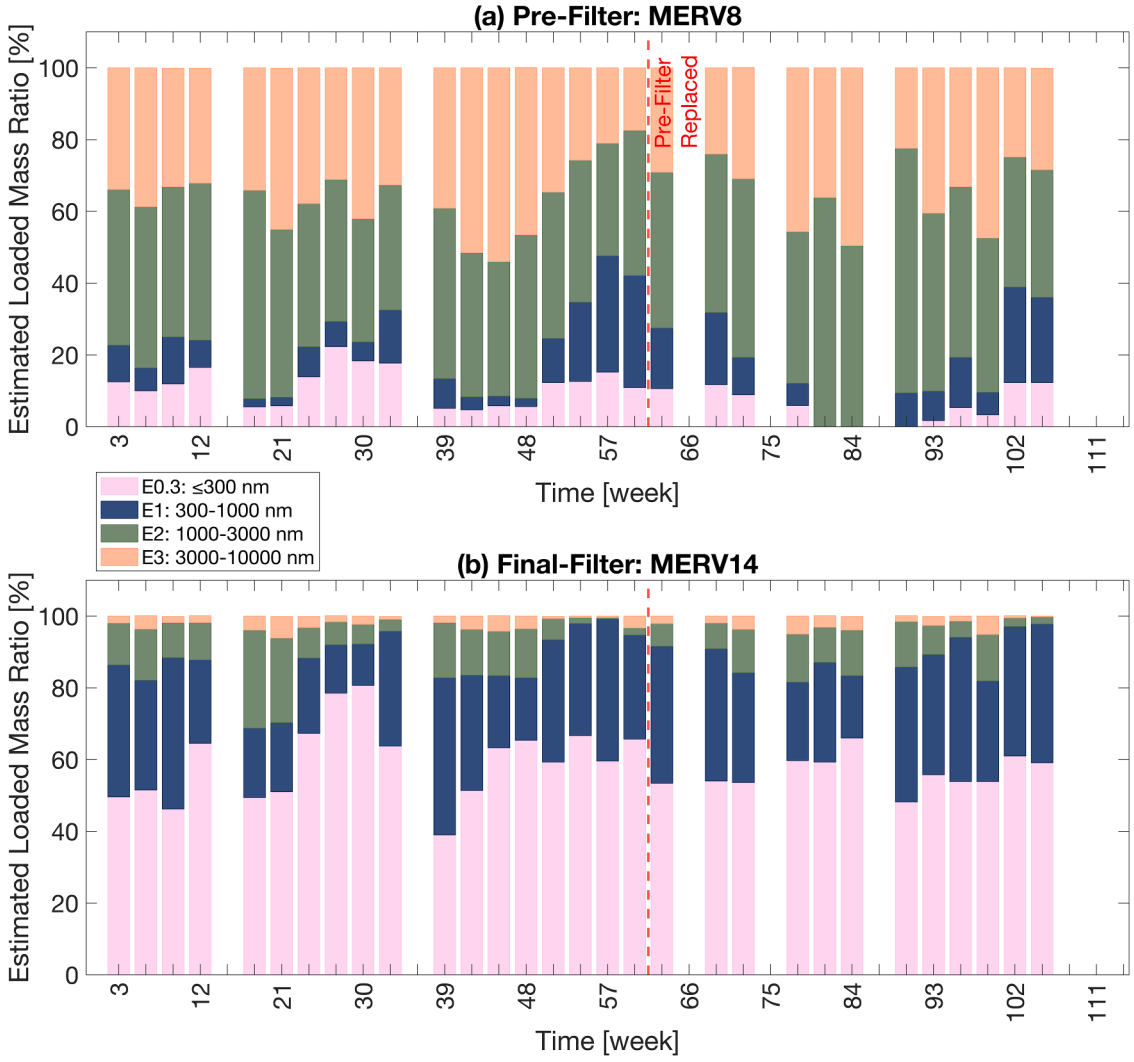

Fig. 11. Weekly filter mass gain ratios for particle size fractions (E0.3, E1, E2, and E3) in Duct 1 during the two-year outdoor aerosol aging period. Panel (a) shows the MERV8 pre-filter, and panel (b) shows the MERV14 final-filter. In each panel, the stacked bars represent the percentage contribution of filter mass gain attributed to the integrated particle mass of E0.3 (≤300 nm; light pink), E1 (300–1000 nm; blue), E2 (1000–3000 nm; green), and E3 (3000–10,000 nm; dark pink) size fractions. Size fraction definitions follow ANSI/ASHRAE Standard 52.2–2017, with the addition of E0.3 to include particles ≤300 nm. Dashed red vertical lines indicate replacement of the MERV8 pre-filter at week 60.

low-volatility gas-phase species likely partition onto deposited particles on the filter media, contributing to filter mass over time but not being captured by SMPS-OPS measurements. In addition, ozone-initiated reactions with squalene and terpenes on filter surfaces can generate secondary aerosol mass, further increasing filter loading beyond that estimated from SMPS-OPS measurements alone [30,126].

Atmospheric aerosol particles larger than $D_{em(o)} = 100$ nm often exhibit moderate to high hygroscopicity, particularly in regions with strong secondary aerosol production (e.g., sulfate-rich environments), with reported hygroscopic fractions reaching up to 61% for accumulation-mode particles ($D_{em(o)} \sim 265$ nm) in urban settings [83–88]. As a result, particles deposited on filters can undergo substantial mass growth due to water uptake under elevated RH conditions. Beyond direct water condensation, prolonged exposure to high humidity (typically >70–80% RH) can also promote bacterial and fungal cell growth on filter media, further contributing to mass accumulation over time [124].

To better understand how different particle size fractions contribute to total mass loading, a comparative analysis (Figs. 11–13) was conducted using SMPS-OPS data to estimate the relative contributions of E0.3 (≤300 nm), E1 (300–1000 nm), E2 (1000–3000 nm), and E3 (3000–10,000 nm) size fractions to the total sub-10,000 nm accumulated mass. The data gaps in Figs. 11–13 correspond to weeks with insufficient data to reliably compute size-fractionated mass gain ratios across the 10–10,000 nm particle size range, primarily due to instrument malfunctions, data corruption, or periods of instrument unavailability. Fig. 11 shows that mass accumulation on the MERV8 pre-filter is dominated by coarse particles, with the E3 and E2 fractions consistently accounting for more than 80% of the total mass, while sub-micron fractions (E0.3 and E1) contribute negligibly. In contrast, the MERV14 final-filter exhibits a markedly different loading profile, with mass gain driven primarily by fine and ultrafine particles; the E0.3 and E1 fractions together frequently exceed 80% of the total mass, with the ≤300 nm fraction alone often exceeding 50% (Fig. 12) Similarly, the MERV13 final-filter shows mass accumulation dominated by E0.3 and E1 particle fractions, reflecting the effective removal of coarse particles by upstream filtration.

The MERV8 final-filter (Fig. 13) exhibits a distinct loading behavior compared to the MERV8 pre-filter. The pre-filter mass is dominated by coarse particles (E3 and E2), whereas the final-filter shows contributions from finer particle fractions, including E0.3 (≤300 nm) and E1 (300–1000 nm), along with E2 (1000–3000 nm). Because both filters in

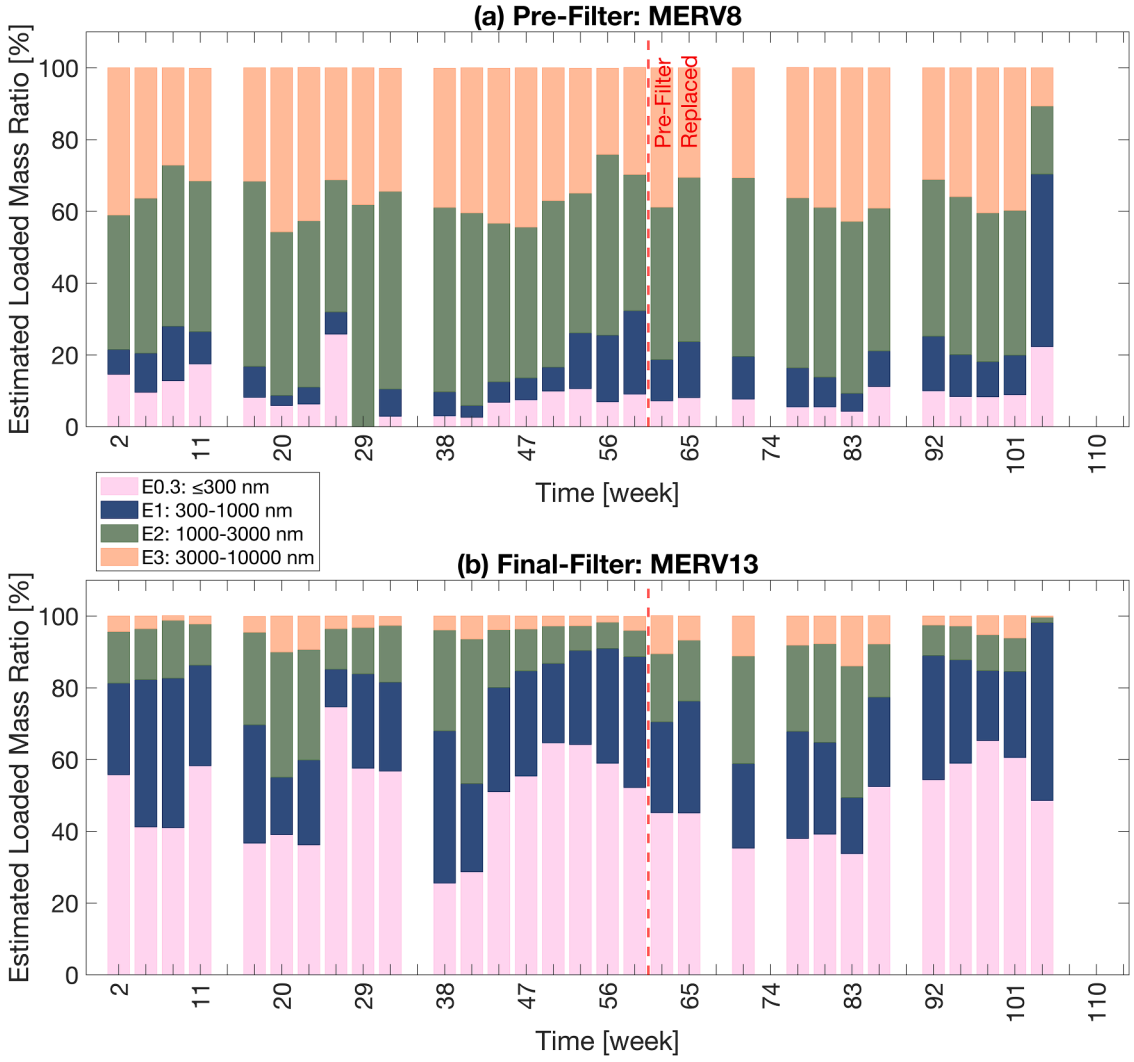

Fig. 12. Weekly filter mass gain ratios for particle size fractions (E0.3, E1, E2, and E3) in Duct 2 during the two-year outdoor aerosol aging period. Panel (a) shows the MERV8 pre-filter, and panel (b) shows the MERV13 final-filter. In each panel, the stacked bars represent the percentage contribution of filter mass gain attributed to the integrated particle mass of E0.3 (≤300 nm; light pink), E1 (300–1000 nm; blue), E2 (1000–3000 nm; green), and E3 (3000–10,000 nm; dark pink) size fractions. Size fraction definitions follow ANSI/ASHRAE Standard 52.2–2017, with the addition of E0.3 to include particles ≤300 nm. Dashed red vertical lines indicate replacement of the MERV 8 pre-filter at week 60.

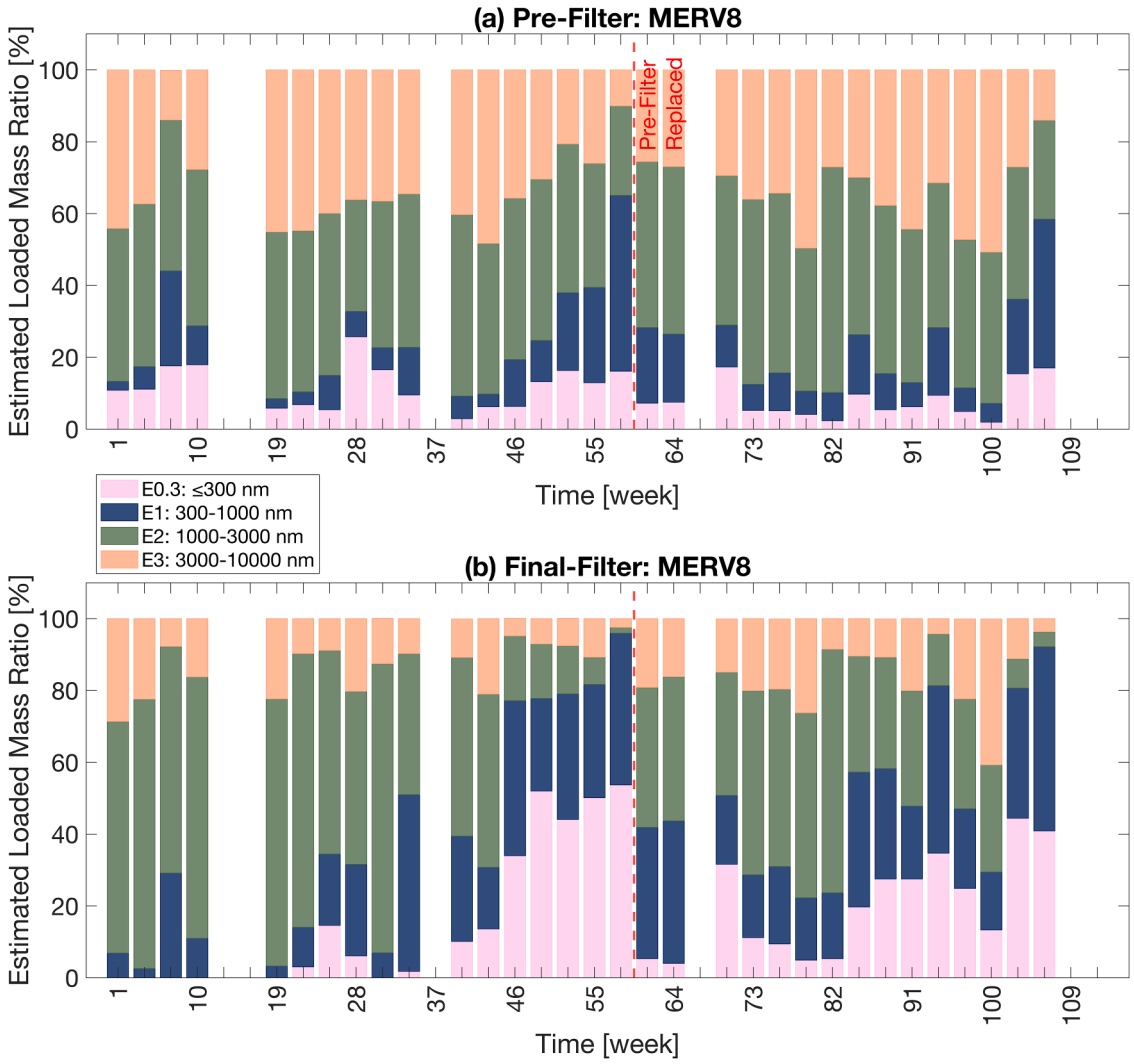

Fig. 13. Weekly filter mass gain ratios for particle size fractions (E0.3, E1, E2, and E3) in Duct 3 during the two-year outdoor aerosol aging period. Panel (a) shows the MERV8 pre-filter, and panel (b) shows the MERV8 final-filter. In each panel, the stacked bars represent the percentage contribution of filter mass gain attributed to the integrated particle mass of E0.3 (≤300 nm; light pink), E1 (300–1000 nm; blue), E2 (1000–3000 nm; green), and E3 (3000–10,000 nm; dark pink) size fractions. Size fraction definitions follow ANSI/ASHRAE Standard 52.2–2017, with the addition of E0.3 to include particles ≤300 nm. Dashed red vertical lines indicate replacement of the MERV 8 pre-filter at week 60.

this configuration are MERV8, the upstream pre-filter removes a large fraction of coarse particles (3000–10,000 nm), allowing sub-3000 nm particles to penetrate and accumulate on the downstream filter. As the pre-filter loads over time, enhanced removal of larger particles due to dust cake formation further reduces coarse particle transport, increasing the relative contribution of fine and ultrafine particles to the final-filter mass. Consistent with these observations, Waring et al. (2008) [32] reported that pre-filters (MERV6–8) effectively remove coarse particles while allowing 80–90% of sub-micron particles to penetrate to downstream filters. As a result, mass accumulation on secondary final-filters is slower but dominated by finer particle fractions, which tend to form denser dust cakes than the coarse deposits observed on pre-filters, as reported in previous studies [34,43,76,127,128]. These findings highlight a key limitation of current laboratory testing protocols (e.g., ANSI/ASHRAE Standard 52.2–2017 [48]), which rely on coarse test dusts (e.g., ISO 12103–1 [129,130]) that do not fully represent the mass-loading characteristics of fine particles on high-efficiency filters. The present results underscore the need to incorporate fine and ultrafine particle loading into standardized tests to better predict the service life and real-world performance of final-stage HVAC filters [129,131].

4. Conclusions

This two-year in-situ evaluation, enabled by a custom-built, full-scale HVAC filter test rig designed to expose filters to outdoor aerosol conditions, demonstrates that HVAC filter performance evolves substantially under continuous atmospheric aerosol loading. Across all ducts, MERV8 pre-filters exhibited exponential increases in ΔP driven by outdoor aerosol deposition, while downstream final-filters contributed comparatively little to total airflow resistance. Mechanical filters, including both MERV8 and MERV14 final-filters, showed stable or increasing filtration efficiency over time, whereas the MERV13 electret final-filter experienced pronounced efficiency loss across the 300–1000 nm (E1) range. These divergent aging trajectories illustrate that laboratory-rated performance does not necessarily predict long-term in-service behavior and highlight the usefulness of the in-situ MERV framework for resolving temporal shifts in filtration efficiency relevant to both HVAC energy consumption and exposure reduction.

The in-situ MERV results further reveal that mechanical filters can exhibit substantial gains in filtration efficiency during aging, while electret media may undergo rapid deterioration due to charge decay accelerated by humid, particle-rich outdoor air. Size-resolved particle

measurements revealed distinct mass loading trajectories by filter type and position: MERV8 pre-filters accumulated mass dominated by coarse particles, whereas final-filters were loaded predominantly by fine and ultrafine particles, with total gravimetric mass gain increasing with final-filter MERV rating. These contrasting loading profiles reflect the selective particle penetration imposed by upstream pre-filtration and underscore a key limitation of current standardized laboratory loading protocols, which rely on coarse test dusts that do not adequately represent the fine and ultrafine particle loading conditions encountered by final-filters in real-world two-stage filtration systems. Under constant airflow operation, weekly fan energy consumption increased progressively alongside rising filter ΔP, with the magnitude and rate of increase varying by filter type and fan efficiency. These findings have practical implications for filtration strategies in mechanically ventilated buildings, particularly for optimizing filter replacement scheduling and predicting long-term energy penalties associated with filter aging.

Several limitations should be considered when interpreting these results. Only one unit of each filter make and model was tested, and performance may vary across products or manufacturers. Results reflect the operating conditions and outdoor aerosol characteristics specific to the test rig and climatic region, and different volumetric airflow rates, blower types, or outdoor air pollution conditions could alter aging behavior. Moreover, episodic air pollution events such as wildfires or dust storms can introduce substantially different outdoor aerosol loading rates, size distributions, and chemical compositions, which may further alter filter aging behavior and performance. Notably, the in-situ MERV calculation differs from the standardized method defined in ANSI/ASHRAE Standard 52.2–2017 and may result in deviations from standard MERV classifications. Despite these limitations, this study provides a uniquely comprehensive, multi-year dataset illustrating the dynamic nature of HVAC filter aging under real-world outdoor aerosol exposure and highlights the need for continued research, improved monitoring approaches, and next-generation filtration technologies to ensure robust indoor air quality, energy efficiency, and system longevity.

CRediT authorship contribution statement

Chunxu Huang: Writing – review & editing, Writing – original draft, Visualization, Validation, Methodology, Investigation, Funding acquisition, Formal analysis, Data curation. **Brandon E. Boor:** Writing – review & editing, Writing – original draft, Visualization, Validation, Supervision, Software, Resources, Project administration, Methodology, Investigation, Funding acquisition, Formal analysis, Data curation, Conceptualization.

Declaration of competing interest

The authors declare that they have no conflict of interest.

Acknowledgments

This work was supported by the American Society of Heating, Refrigerating, and Air-Conditioning Engineers (ASHRAE) under Grant RP-1734 (to B.E.B.) and by an ASHRAE Graduate Student Grant-In-Aid Award (to C.H.). The authors are grateful for the support of the ASHRAE RP-1734 Project Monitoring Subcommittee: Paolo Tronville, Geoff Crosby, Bruce McDonald, Tom Justice, and Brian Krafthefer. The authors also thank Dr. Nusrat Jung, Hajin Park, Iane Loise Moreira Gomes, Laura Ajala, Brian H. Magnuson, Ekpeme Gbemiye-Etta, Caio K. Sugane Hamada, Susan L. Huster, and Ta-Kuan Chuang for their assistance and support.

Supplementary materials

Supplementary material associated with this article can be found in the online version, at doi:10.1016/j.buildenv.2026.114596.

Data availability

Data will be made available on request.

References

[1] X. Ding, H. Lu, J. Jiang, A. Tasoglou, A.D. Shah, N. Jung, Real-time indoor sensing of volatile organic compounds during building disinfection events via photoionization detection and proton transfer reaction mass spectrometry, Build. Environ. 246 (2023) 108050, https://doi.org/10.1016/j.buildenv.2023.110953.
[2] J. Namieĝnik, T. Górecki, B. KozdroĆ-ZabiegaĄa, J. ăukasiak, Indoor air quality (IAQ), pollutants, their sources and concentration levels, Build. Environ. 27 (3) (1992) 339–356, https://doi.org/10.1016/0360-1323(92)90034-M.
[3] S. Kamaruzzaman, N.A. Sabrani, The effect of Indoor Air Quality (IAQ) towards occupants' psychological performance in office buildings, J. Rekabentuk Dan Binaan 4 (2011) 49–61.
[4] R.D. Brook, S. Rajagopalan, C.A. Pope, J.R. Brook, A. Bhatnagar, A.V. Diez-Roux, F. Holguin, Y. Hong, R.V. Luepker, M.A. Mittleman, A. Peters, D. Siscovick, S. C. Smith, L. Whitsel, J.D. Kaufman, Particulate matter air pollution and cardiovascular disease: an update to the scientific statement from the American Heart Association, Circulation. 121 (2010) 2331–2378, https://doi.org/10.1161/CIR.0b013e3181dbece1.
[5] K.W. Tham, Indoor air quality and its effects on humans-a review of challenges and developments in the last 30 years, Energy Build. 130 (2016) 637–650, https://doi.org/10.1016/j.enbuild.2016.08.071.
[6] Z. Deng, B. Dong, X. Guo, J. Zhang, Impact of indoor air quality and multi-domain factors on human productivity and physiological responses: a comprehensive review, Indoor Air (2024) 584960, https://doi.org/10.1155/2024/5584960.
[7] V. Van Tran, D. Park, Y.C. Lee, Indoor air pollution, related human diseases, and recent trends in the control and improvement of indoor air quality, Int. J. Environ. Res. Public Health. 17 (8) (2020) 2927, https://doi.org/10.3390/ijerph17082927.
[8] W. Wang, R. Ooka, H. Kikumoto, W. Oh, M. Han, Influence of various factors on indoor/outdoor pollen concentration ratio based on experimental research: a review, Build. Environ. 219 (2022) 109154, https://doi.org/10.1016/j.buildenv.2022.109154.
[9] D.A. Sterling, R.D. Lewis, Pollen and fungal spores indoor and outdoor of mobile homes, Ann. Allergy Asthma Immunol. 80 (1998) 279–285, https://doi.org/10.1016/S1081-1206(10)62971-7.
[10] I. Goh, J.P. Obbard, S. Viswanathan, Y. Huang, Airborne bacteria and fungal spores in the indoor environment. A case study in Singapore, Acta. Biotechnol. 20 (2000) 67–73, https://doi.org/10.1002/abio.370200111.
[11] P.R. Tumminello, R.C. James, S. Kruse, A. Kawasaki, A. Cooper, I. Guadalupe-Diaz, K.L. Zepeda, D.R. Crocker, K.J. Mayer, J.S. Sauer, C. Lee, K.A. Prather, J. H. Slade, Evolution of sea spray aerosol particle phase state across a phytoplankton bloom, ACS Earth Space Chem. 5 (2021) 2995–3007, https://doi.org/10.1021/acsearthspacechem.1c00186.
[12] P.R. Tumminello, R. Niles, V. Valdez, C.K. Madawala, D.K. Gamage, K.A. Kimble, R.J. Leibensperger, C. Huang, C. Kaluarachchi, J. Dinasquet, F. Malfatti, C. Lee, G. B. Deane, M.D. Stokes, E. Stone, A. Tivanski, K.A. Prather, B.E. Boor, J.H. Slade, Size-dependent nascent sea spray aerosol bounce fractions and estimated viscosity: the role of divalent cation enrichment, surface tension, and the kelvin effect, Environ. Sci. Technol. 58 (44) (2024) 19666–19678, https://doi.org/10.1021/acs.est.4c04312.
[13] K. O'Dell, B. Ford, J. Burkhardt, S. Magzamen, S.C. Anenberg, J. Bayham, E. V. Fischer, J.R. Pierce, Outside in: the relationship between indoor and outdoor particulate air quality during wildfire smoke events in western US cities, Environment. Res. 1 (2023) 015003, https://doi.org/10.1088/2752-5309/ac7d69.
[14] J. Jiang, N. Jung, B.E. Boor, Using building energy and smart thermostat data to evaluate indoor ultrafine particle source and loss processes in a net-zero energy house, ACS ES&T Eng. 1 (4) (2021) 780–793, https://doi.org/10.1021/acsestengg.1c00002.
[15] S.S. Patra, J. Liu, J. Jiang, X. Ding, C. Huang, C. Keech, G. Steiner, P.S. Stevens, N. Jung, B.E. Boor, Rapid nucleation and growth of indoor atmospheric nanocluster aerosol during the use of scented volatile chemical products in residential buildings, ACS ES&T Air. 1 (10) (2024) 1276–1293, https://doi.org/10.1021/acsestair.4c00118.
[16] S.S. Patra, J. Jiang, X. Ding, C. Huang, E.K. Reidy, V. Kumar, P. Price, C. Keech, G. Steiner, P. Stevens, N. Jung, B.E. Boor, Dynamics of nanocluster aerosol in the indoor atmosphere during gas cooking, PNAS Nexus. 3 (2) (2024) 1–11, https://doi.org/10.1093/pnasnexus/pgae044.
[17] J. Jiang, X. Ding, K.P. Isaacson, A. Tasoglou, H. Huber, A.D. Shah, N. Jung, B. E. Boor, Ethanol-based disinfectant sprays drive rapid changes in the chemical composition of indoor air in residential buildings, J. Hazardous Mater. Lett. 2 (2021) 100042, https://doi.org/10.1016/j.hazl.2021.100042.
[18] J. Jiang, X. Ding, S.S. Patra, J.N. Cross, C. Huang, V. Kumar, P. Price, E.K. Reidy, A. Tasoglou, H. Huber, P.S. Stevens, B.E. Boor, N. Jung, Siloxane emissions and exposures during the use of hair care products in buildings, Environ. Sci. Technol. 57 (2023) 19999–20009, https://doi.org/10.1021/acs.est.3c05156.
[19] J. Liu, J. Jiang, X. Ding, S.S. Patra, J.N. Cross, C. Huang, V. Kumar, P. Price, E. K. Reidy, A. Tasoglou, H. Huber, P.S. Stevens, B.E. Boor, N. Jung, Real-time

evaluation of terpene emissions and exposures during the use of scented wax products in residential buildings with PTR-TOF-MS, Build. Environ. 255 (2024) 111314, https://doi.org/10.1016/j.buildenv.2024.111314.
[20] C.M.F. Rosales, J. Jiang, A. Lahib, B.P. Bottorff, E.K. Reidy, V. Kumar, A. Tasoglou, H. Huber, S. Dusanter, A. Tomas, B.E. Boor, P.S. Stevens, Chemistry and human exposure implications of secondary organic aerosol production from indoor terpene ozonolysis, Sci. Adv. 8 (8) (2022) 9156, https://doi.org/10.1126/sciadv.abj9156.
[21] S.S. Patra, T. Wu, D.N. Wagner, J. Jiang, B.E. Boor, Real-time measurements of fluorescent aerosol particles in a living laboratory office under variable human occupancy and ventilation conditions, Build. Environ. 205 (2021) 108249, https://doi.org/10.1016/j.buildenv.2021.108249.
[22] P. Azimi, B. Stephens, HVAC filtration for controlling infectious airborne disease transmission in indoor environments: predicting risk reductions and operational costs, Build. Environ. 70 (2013) 150–160, https://doi.org/10.1016/j.buildenv.2013.08.025.
[23] D.M. Lunderberg, Y. Liang, B.C. Singer, J.S. Apte, W.W. Nazaroff, A.H. Goldstein, Assessing residential $PM_{2.5}$ concentrations and infiltration factors with high spatiotemporal resolution using crowdsourced sensors, Proc. Natl. Acad. Sci. U.S.A. 120 (50) (2023) e2308832120, https://doi.org/10.1073/pnas.2308832120.
[24] J. Taylor, C. Shrubsole, M. Davies, P. Biddulph, P. Das, I. Hamilton, S. Vardoulakis, A. Mavrogianni, B. Jones, E. Oikonomou, The modifying effect of the building envelope on population exposure to $PM_{2.5}$ from outdoor sources, Indoor Air. 24 (2014) 639–651, https://doi.org/10.1111/ina.12116.
[25] N.W. May, C. Dixon, D.A. Jaffe, Impact of wildfire smoke events on indoor air quality and evaluation of a low-cost filtration method, Aerosol Air Qual. Res. 21 (2021) 210046, https://doi.org/10.4209/aaqr.210046.
[26] T. Mangin, Z. Barrett, Z. Palmer, D. Tang, S. Nielson, D. Sleeth, K. Kelly, Understanding the effect of outdoor pollution episodes and HVAC type on indoor air quality, Build. Environ. 278 (2025) 112978, https://doi.org/10.1016/j.buildenv.2025.112978.
[27] J. Cox, K. Isiugo, P. Ryan, S.A. Grinshpun, M. Yermakov, C. Desmond, R. Jandarov, S. Vesper, J. Ross, S. Chillrud, K. Dannemiller, T. Reponen, Effectiveness of a portable air cleaner in removing aerosol particles in homes close to highways, Indoor Air. 28 (2018) 818–827, https://doi.org/10.1111/ina.12502.
[28] B. Stephens, Building design and operational choices that impact indoor exposures to outdoor particulate matter inside residences, Sci. Technol. Built Environ. 21 (2015) 3–13, https://doi.org/10.1080/10789669.2014.961849.
[29] L. Tofful, S. Canepari, T. Sargolini, C. Perrino, Indoor air quality in a domestic environment: combined contribution of indoor and outdoor PM sources, Build. Environ. 202 (2021) 108050, https://doi.org/10.1016/j.buildenv.2021.108050.
[30] P. Zhao, J.A. Siegel, R.L. Corsi, Ozone removal by HVAC filters, Atmos. Environ. 41 (2007) 3151–3160, https://doi.org/10.1016/j.atmosenv.2006.06.059.
[31] T. Wu, A. Tasoglou, D.N. Wagner, J. Jiang, H.J. Huber, P.S. Stevens, N. Jung, B. E. Boor, Modern buildings act as a dynamic source and sink for urban air pollutants, Cell Report. Sustain. 1 (2024) 100103, https://doi.org/10.1016/j.crsus.2024.100103.
[32] M.S. Waring, J.A. Siegel, Particle loading rates for HVAC filters, heat exchangers, and ducts, Indoor Air. 18 (2008) 209–224, https://doi.org/10.1111/j.1600-0668.2008.00518.x.
[33] L. Jung, Impact of Air-Filter Condition on HVAC (Heating, Ventilation, and Air Conditioning) Equipment, Report No. ORNL/TM-9894, Oak Ridge National Laboratory, Oak Ridge, TN, 1987, https://doi.org/10.2172/814094.
[34] W. Poon, B. Liu, A bimodal loading test for engine and general purpose air cleaning filters, SAE Tech. Paper (1997) 970674, https://doi.org/10.4271/970674.
[35] J.F. Montgomery, S.I. Green, S.N. Rogak, Impact of relative humidity on HVAC filters loaded with hygroscopic and non-hygroscopic particles, Aerosol Sci. Technol. 49 (2015) 322–331, https://doi.org/10.1080/02786826.2015.1026433.
[36] J.K. Lee, S.C. Kim, B.Y.H. Liu, Effect of bi-modal aerosol mass loading on the pressure drop for gas cleaning industrial filters, Aerosol Sci. Technol. 35 (2001) 805–814, https://doi.org/10.1080/027868201753227352.
[37] R.D. Rivers, D.J. Murphy Jr. Air filter performance under variable air volume conditions, ASHRAE Trans. 106 (2000) 131, https://www.proquest.com/scholarly-journals/air-filterperformance-under-variable-volume/docview/192519486/se-2.
[38] M. Tang, K. Owen, A. Novoselac, Evaluating test method of air cleaning devices for ozone removal (ASHRAE RP-1579), Sci. Technol. Built Environ. 28 (2022) 886–895, https://doi.org/10.1080/23744731.2022.2080109.
[39] A.D. Schwarz, L. König, J. Meyer, A. Dittler, Impact of water droplet and humidity interaction with soluble particles on the operational performance of surface filters in gas cleaning applications, J. Aerosol Sci. 142 (2020) 105523, https://doi.org/10.1016/j.jaerosci.2020.105523.
[40] X. Tian, Q. Ou, J. Liu, Y. Liang, D.Y.H. Pui, Particle loading characteristics of a two-stage filtration system, Sep. Purif. Technol. 215 (2019) 351–359, https://doi.org/10.1016/j.seppur.2019.01.033.
[41] S. Li, D.R. Chen, F. Zhou, S.C. Chen, Effects of relative humidity and particle hygroscopicity on the initial efficiency and aging characteristics of electret HVAC filter media, Build. Environ. 171 (2020) 106669, https://doi.org/10.1016/j.buildenv.2020.106669.
[42] Q. Wang, X. Lin, D.R. Chen, Effect of dust loading rate on the loading characteristics of high efficiency filter media, Powder Technol. 287 (2016) 20–28, https://doi.org/10.1016/j.powtec.2015.09.032.
[43] T. Valmari, M. Lehtimäki, A. Taipale, Filter clogging by bimodal aerosol, Aerosol Sci. Technol. 40 (2006) 255–260, https://doi.org/10.1080/02786820500543282.
[44] A.F. Miguel, Effect of air humidity on the evolution of permeability and performance of a fibrous filter during loading with hygroscopic and non-hygroscopic particles, J. Aerosol Sci. 34 (2003) 783–799, https://doi.org/10.1016/S0021-8502(03)00027-2.
[45] C. Liu, Z. Dai, B. He, Q.F. Ke, The effect of temperature and humidity on the filtration performance of electret melt-blown nonwovens, Materials 13 (21) (2020) 4774, https://doi.org/10.3390/ma13214774.
[46] P.K. Giffin, M.S. Parsons, R.J. Unz, C.A. Waggoner, Large-scale generic test stand for testing of multiple configurations of air filters utilizing a range of particle size distributions, Rev. Scientif. Instrument. 83 (2012) 055105, https://doi.org/10.1063/1.4717671.
[47] A. Bastani, C.S. Lee, F. Haghighat, C. Flaherty, N. Lakdawala, Assessing the performance of air cleaning devices - a full-scale test method, Build. Environ. 45 (2010) 143–149, https://doi.org/10.1016/j.buildenv.2009.05.008.
[48] ASHRAE, Method of Testing General Ventilation Air-Cleaning Devices for Removal Efficiency by Particle Size, in: ANSI/ASHRAE 52.2-2017, Atlanta, GA, 2017.
[49] Y. Zhang, T. Li, J.A. Siegel, Investigating the impact of filters on long-term particle concentration measurements in residences (RP-1649), Sci. Technol. Built. Environ. 26 (2020) 1037–1047, https://doi.org/10.1080/23744731.2020.1778402.
[50] T. Li, J. Siegel, Laboratory performance of new and used residential HVAC filters: comparison to field results (RP-1649), Sci. Technol. Built Environ. 26 (2020) 844–855, https://doi.org/10.1080/23744731.2020.1738871.
[51] P.C. Raynor, S.J. Chae, Dust loading on electrostatically charged filters in a standard test and a real HVAC system, Filtr. Sep. 40 (3) (2003) 35–39, https://doi.org/10.1016/S0015-1882(03)80068-X.
[52] T. Wu, B.E. Boor, Urban aerosol size distributions: a global perspective, Atmos. Chem. Phys. 21 (2021) 8883–8914, https://doi.org/10.5194/acp-21-8883-2021.
[53] M.W. First, S.N. Rudnick, X. Yan, Use of alternative liquids in laskin nozzle generated aerosols for filter testing, Am. Ind. Hyg. Assoc. J. 53 (1992) 242–247, https://doi.org/10.1080/15298669291359591.
[54] B. Stephens, A. Novoselac, J.A. Siegel, The effects of filtration on pressure drop and energy consumption in residential HVAC systems (RP-1299), HVAC&R Res. 16 (2010) 273–294, https://doi.org/10.1080/10789669.2010.10390905.
[55] M. Zaatari, A. Novoselac, J. Siegel, The relationship between filter pressure drop, indoor air quality, and energy consumption in rooftop HVAC units, Build. Environ. 73 (2014) 151–161, https://doi.org/10.1016/j.buildenv.2013.12.010.
[56] J.E. Yit, B.T. Chew, Y.H. Yau, A review of air filter test standards for particulate matter of general ventilation, Build. Servic. Eng. Res. Technol. 41 (2020) 758–771, https://doi.org/10.1177/0143624420915626.
[57] B. Stephens, J.A. Siegel, Ultrafine particle removal by residential heating, ventilating, and air-conditioning filters, Indoor Air. 23 (2013) 488–497, https://doi.org/10.1111/ina.12045.
[58] T. Fazli, Y. Zeng, B. Stephens, Fine and ultrafine particle removal efficiency of new residential HVAC filters, Indoor Air. 29 (2019) 656–669, https://doi.org/10.1111/ina.12566.
[59] T. Li, J.A. Siegel, In situ efficiency of filters in residential central HVAC systems, Indoor Air. 30 (2) (2020) 315–325, https://doi.org/10.1111/ina.12633.
[60] M. Alavy, J.A. Siegel, In-situ effectiveness of residential HVAC filters, Indoor Air. 30 (2020) 156–166, https://doi.org/10.1111/ina.12617.
[61] M. Alavy, T. Li, J.A. Siegel, Energy use in residential buildings: analyses of high-efficiency filters and HVAC fans, Energy Build. 209 (2020) 109697, https://doi.org/10.1016/j.enbuild.2019.109697.
[62] M. Alavy, J.A. Siegel, IAQ and energy implications of high efficiency filters in residential buildings: a review (RP-1649), Sci. Technol. Built Environ. 25 (2019) 261–271, https://doi.org/10.1080/23744731.2018.1526012.
[63] ASHRAE. Standard Methods for Air Velocity and Airflow Measurement, in: ANSI/ASHRAE, Standard 41.2-2022, Atlanta, GA, 2022.
[64] M. Yamada, M Takaya, I. Ogura, Performance evaluation of newly developed portable aerosol sizers used for nanomaterial aerosol measurements, Indu. Hea. 53 (6) (2015) 511–516, https://doi.org/10.2486/indhealth.2014-0243.
[65] E. Vo, M. Horvatin, Z. Zhuang, Performance comparison of field portable instruments to the scanning mobility particle sizer using monodispersed and polydispersed sodium chloride aerosols, Ann. Work Expo. Health. 62 (2018) 711–720, https://doi.org/10.1093/annweh/wxy036.
[66] W. Hoeflinger, $PM_{2.5}$ separation efficiency and energy assessment for cleanable dust- and oil-water soluble mist filter media, Proc. Safe. Environment. Protect. 197 (2025) 106950, https://doi.org/10.1016/j.psep.2025.106950.
[67] Eurovent 4/21 – 2019, Eurovent Industry Recommendation / Code of Good Practice: Energy Efficiency Evaluation of Air Filters for General Ventilation Purposes, fourth ed., Eurovent Association, Brussels, 2019. https://www.eurovent.eu/publications/eurovent-4-21-2019-energyefficiency-evaluation-of-air-filters-for-general-ventilation-purposes-fourth-edition/.
[68] J.F. Montgomery, S.I. Green, S.N. Rogak, K. Bartlett, Predicting the energy use and operation cost of HVAC air filters, Energy Build. 47 (2012) 643–650, https://doi.org/10.1016/j.enbuild.2012.01.001.
[69] B. Considine, J. Gallagher, P. Kumar, A. McNabola, Long-term assessment of energy consumption reduction in a building ventilation system with passive particulate matter control technology in the fresh air intake, Energy Build. 309 (2024) 114067, https://doi.org/10.1016/j.enbuild.2024.114067.
[70] D.T. Morgan, T. Daly, J. Gallagher, A. McNabola, Reducing energy consumption and increasing filter life in HVAC systems using an aspiration efficiency reducer:

long-term performance assessment at full-scale, J. Build. Eng. 12 (2017) 267–274, https://doi.org/10.1016/j.jobe.2017.06.014.
[71] H. Zhao, B. Stephens, Using portable particle sizing instrumentation to rapidly measure the penetration of fine and ultrafine particles in unoccupied residences, Indoor Air. 27 (2017) 218–229, https://doi.org/10.1111/ina.12295.
[72] G. Berry, I. Beckman, H. Cho, A comprehensive review of particle loading models of fibrous air filters, J. Aerosol Sci. 167 (2023) 106078, https://doi.org/10.1016/j.jaerosci.2022.106078.
[73] W.C. Hinds, Y. Zhu. Aerosol Technology: Properties, Behavior, and Measurement of Airborne Particles, 3rd ed., John Wiley & Sons, 2022.
[74] W. Poon, B. Liu, Dust loading behavior of engine and general purpose air cleaning filters, SAE Tech. Paper (1997) 970676, https://doi.org/10.4271/970674.
[75] Y. Endo, D.-R. Chen, D.Y.H. Pui, Effects of particle polydispersity and shape factor during dust cake loading on air filters, Powder. Technol. 98 (1998) 241–249, https://doi.org/10.1016/S0032-5910(98)00063-1.
[76] Y. Endo, D.-R. Chen, D.Y.H. Pui, Bimodal aerosol loading and dust cake formation on air filters, Filtr. Sep. 35 (1998) 191–195, https://doi.org/10.1016/S0015-1882(98)91369-6.
[77] S. Lu, C. Bhattarai, V. Samburova, A. Khlystov, Particle size distributions of wildfire aerosols in the western USA, Environ. Sci. Atmos. 5 (2025) 502–516, https://doi.org/10.1039/d5ea00007f.
[78] M. Sillanpää, S. Saarikoski, R. Hillamo, A. Pennanen, U. Makkonen, Z. Spolnik, R. Van Grieken, T. Koskentalo, R.O. Salonen, Chemical composition, mass size distribution and source analysis of long-range transported wildfire smokes in Helsinki, Sci. Total Environ. 350 (2005) 119–135, https://doi.org/10.1016/j.scitotenv.2005.01.024.
[79] T. Shirman, E. Shirman, S. Liu, Evaluation of filtration efficiency of various filter media in addressing wildfire smoke in indoor environments: importance of particle size and composition, Atmosphere. 14 (12) (2023) 1729, https://doi.org/10.3390/atmos14121729.
[80] T.D. Vaden, D. Imre, J. Beránek, M. Shrivastava, A. Zelenyuk, Evaporation kinetics and phase of laboratory and ambient secondary organic aerosol, Proc. Natl. Acad. Sci. U.S.A. 108 (2011) 2190–2195, https://doi.org/10.1073/pnas.1013391108.
[81] J. Wilson, D. Imre, J. Beránek, M. Shrivastava, A. Zelenyuk, Evaporation kinetics of laboratory-generated secondary organic aerosols at elevated relative humidity, Environ. Sci. Technol. 49 (2015) 243–249, https://doi.org/10.1021/es505331d.
[82] J.F. Montgomery, S.N. Rogak, S.I. Green, Y. You, A.K. Bertram, Structural change of aerosol particle aggregates with exposure to elevated relative humidity, Environ. Sci. Technol. 49 (2015) 12054–12061, https://doi.org/10.1021/acs.est.5b03157.
[83] G.P. Almeida, A.T. Bittencourt, M.S. Evangelista, M.S. Vieira-Filho, A. Fornaro, Characterization of aerosol chemical composition from urban pollution in Brazil and its possible impacts on the aerosol hygroscopicity and size distribution, Atmos. Environ. 202 (2019) 149–159, https://doi.org/10.1016/j.atmosenv.2019.01.024.
[84] A. Yu, X. Shen, Q. Ma, J. Lu, X. Hu, Y. Zhang, Q. Liu, L. Liang, L. Liu, S. Liu, H. Tong, H. Che, X. Zhang, J. Sun, Size-resolved hygroscopicity and volatility properties of ambient urban aerosol particles measured by a volatility hygroscopicity tandem differential mobility analyzer system in Beijing, Atmos. Chem. Phys. 25 (2025) 3389–3412, https://doi.org/10.5194/acp-25-3389-2025.
[85] N. Kim, S.S. Yum, M. Park, J.S. Park, H.J. Shin, J.Y. Ahn, Hygroscopicity of urban aerosols and its link to size-resolved chemical composition during spring and summer in Seoul, Korea, Atmos. Chem. Phys. 20 (2020) 11245–11262, https://doi.org/10.5194/acp-20-11245-2020.
[86] S. Deshmukh, L. Poulain, B. Wehner, S. Henning, J.E. Petit, P. Fombelle, O. Favez, H. Herrmann, M. Pöhlker, External particle mixing influences hygroscopicity in a sub-urban area, Atmos. Chem. Phys. 25 (2025) 741–758, https://doi.org/10.5194/acp-25-741-2025.
[87] J. Enroth, J. Mikkilä, Z. Németh, M. Kulmala, I. Salma, Wintertime hygroscopicity and volatility of ambient urban aerosol particles, Atmos. Chem. Phys. 18 (2018) 4533–4548, https://doi.org/10.5194/acp-18-4533-2018.
[88] T.V. Vu, Z. Shi, R.M. Harrison, Estimation of hygroscopic growth properties of source-related sub-micrometre particle types in a mixed urban aerosol, NPJ Clim. Atmos. Sci. 4 (21) (2021) 2397–3722, https://doi.org/10.1038/s41612-021-00175-w.
[89] B. Stephens, J.A. Siegel, A. Novoselac, Energy implications of filtration in residential and light-commercial buildings (RP-1299), ASHRAE Trans. 116 (1) (2010) 346–357.
[90] B. Stephens, J.A. Siegel, Comparison of test methods for determining the particle removal efficiency of filters in residential and light-commercial central HVAC systems, Aerosol Sci. Technol. 46 (2012) 504–513, https://doi.org/10.1080/02786826.2011.642825.
[91] P Kulkarni, PA Baron, K Willeke. Aerosol Measurement: Principles, Techniques, and Applications, 3rd ed., John Wiley & Sons, Inc, 2011.
[92] H. Destaillats, W. Chen, M.G. Apte, N. Li, M. Spears, J. Almosni, G. Brunner, J. J. Zhang, W.J. Fisk, Secondary pollutants from ozone reactions with ventilation filters and degradation of filter media additives, Atmos. Environ. 45 (2011) 3561–3568, https://doi.org/10.1016/j.atmosenv.2011.03.066.
[93] G. Bekö, G. Tamás, O. Halás, G. Clausen, C.J. Weschler, in: Ultra-fine particles as indicators of the generation of oxidized products on the surface of used air filters, roceedings of the Indoor Air 2005 Conference, Beijing, China, 2005.
[94] C. Wang, X. Chen, Y. Liu, T. Huang, S. Jiang, Theoretical study of the gas-phase hydrolysis of formaldehyde to produce methanediol and its implication to new particle formation, ACS Omega. 8 (2023) 15467–15478, https://doi.org/10.1021/acsomega.3c00770.
[95] N. Tang, L. Zhang, J. Chen, Y. Pan, H. Xu, C. Wang, Gas-phase aldol condensation of formaldehyde to produce hydroxyacetaldehyde and its implication to new particle formation: a theoretical study, RSC Adv. 14 (2024) 38222–38231, https://doi.org/10.1039/d4ra08063g.
[96] M. Odabasi, R. Seyfioglu, Phase partitioning of atmospheric formaldehyde in a suburban atmosphere, Atmos. Environ. 39 (2005) 5149–5156, https://doi.org/10.1016/j.atmosenv.2005.05.006.
[97] R. Xu, X. Li, H. Dong, D. Lv, N. Kim, S. Yang, W. Wang, J. Chen, M. Shao, S. Lu, Z. Wu, S. Chen, S. Guo, M. Hu, Y. Liu, L. Zeng, Y. Zhang, Field observations and quantifications of atmospheric formaldehyde partitioning in gaseous and particulate phases, Sci. Total Environ. 808 (2022) 152122, https://doi.org/10.1016/j.scitotenv.2021.152122.
[98] M. Hyttinen, P. Pasanen, P. Kalliokoski, Removal of ozone on clean, dusty and sooty supply air filters, Atmos. Environ. 40 (2006) 315–325, https://doi.org/10.1016/j.atmosenv.2005.09.040.
[99] M. Hyttinen, P. Pasanen, M. Björkroth, P. Kalliokoski, Odors and volatile organic compounds released from ventilation filters, Atmos. Environ. 41 (2007) 4029–4039, https://doi.org/10.1016/j.atmosenv.2007.01.029.
[100] M. Hyttinen, P. Pasanen, J. Salo, M. Björ, M. Vartiainen, P. Kalliokoski, Reactions of ozone on ventilation filters, Indoor Built Environ. 12 (3) (2003) 151–158, https://doi.org/10.1177/142032603033362.
[101] R. Bai, C. Tien, Particle detachment in deep bed filtration, J. Colloid Interface Sci. 186 (2) (1997) 307–317, https://doi.org/10.1006/jcis.1996.4663.
[102] L. Ji, J. Pei, W. Liu, Long-term performance of fibrous ventilation/air-cleaner filters for particle removal, Build. Environ. 160 (2019) 106222, https://doi.org/10.1016/j.buildenv.2019.106222.
[103] D.Q. Chang, S.C. Chen, A.R. Fox, A.S. Viner, D.Y.H. Pui, Penetration of sub-50 nm nanoparticles through electret HVAC filters used in residence, Aerosol Sci. Technol. 49 (2015) 966–976, https://doi.org/10.1080/02786826.2015.1086723.
[104] A. Wiedensohler, W. Birmili, A. Nowak, A. Sonntag, K. Weinhold, M. Merkel, B. Wehner, T. Tuch, S. Pfeifer, M. Fiebig, A.M. Fjäraa, E. Asmi, K. Sellegri, R. Depuy, H. Venzac, P. Villani, P. Laj, P. Aalto, J.A. Ogren, E. Swietlicki, P. Williams, P. Roldin, P. Quincey, C. Hüglin, R. Fierz-Schmidhauser, M. Gysel, E. Weingartner, F. Riccobono, S. Santos, C. Grüning, K. Faloon, D. Beddows, R. Harrison, C. Monahan, S.G. Jennings, C.D. O'Dowd, A. Marinoni, H.G. Horn, L. Keck, J. Jiang, J. Scheckman, P.H. McMurry, Z. Deng, C.S. Zhao, M. Moerman, B. Henzing, G. De Leeuw, G. Löschau, S. Bastian, Mobility particle size spectrometers: harmonization of technical standards and data structure to facilitate high quality long-term observations of atmospheric particle number size distributions, Atmos. Meas. Tech. 5 (2012) 657–685, https://doi.org/10.5194/amt-5-657-2012.
[105] M.R. Stolzenburg, P.H. McMurry, Equations governing single and tandem DMA configurations and a new lognormal approximation to the transfer function, Aerosol Sci. Technol. 42 (2008) 421–432, https://doi.org/10.1080/02786820802157823.
[106] A. Wiedensohler, An approximation of the bipolar charge distribution for particles in the submicron size range, J. Aerosol Sci. 19 (3) (1988) 387–389, https://doi.org/10.1016/0021-8502(88)90278-9.
[107] A. Kilic, S. Russell, E. Shim, B. Pourdeyhimi. The charging and stability of electret filters, Fibrous Filter Media, Elsevier Inc, 2017, pp. 95–121, https://doi.org/10.1016/B978-0-08-100573-6.00025-3.
[108] E. Motyl, B. äowkis, Effect of air humidity on charge decay and lifetime of PP electret nonwovens, Fibres Text, East. Eur. 14 (5) (2006) 39–42.
[109] R.R. Cai, H. Lu, L.Z. Zhang, Mechanisms of performance degradation and efficiency improvement of electret filters during neutral particle loading, Powder Technol. 382 (2021) 133–143, https://doi.org/10.1016/j.powtec.2020.12.061.
[110] J. Lee, J. Kim, Material properties influencing the charge decay of electret filters and their impact on filtration performance, Polymers. 12 (3) (2020) 721, https://doi.org/10.3390/polym12030721.
[111] J.H. Ji, G.N. Bae, S.H. Kang, J. Hwang, Effect of particle loading on the collection performance of an electret cabin air filter for submicron aerosols, J. Aerosol Sci. 34 (2003) 1493–1504, https://doi.org/10.1016/S0021-8502(03)00103-4.
[112] M. Tang, S.C. Chen, D.Q. Chang, X. Xie, J. Sun, D.Y.H. Pui, Filtration efficiency and loading characteristics of $PM_{2.5}$ through composite filter media consisting of commercial HVAC electret media and nanofiber layer, Sep. Purif. Technol. 198 (2018) 137–145, https://doi.org/10.1016/j.seppur.2017.03.040.
[113] T. Pistochini, G. Jaeger, C.D. Cappa, R.L. Corsi, Longevity of size-dependent particle removal performance of do-it-yourself box fan air filters, Environ. Sci. Process. Impact. 27 (2024) 1629–1639, https://doi.org/10.1039/d4em00406j.
[114] D. Shi, J. Li, Y. Du, Q. Wu, S. Huang, H. Huang, D. Wu, Influence of relative humidity on the characteristics of filter cake using particle flow code simulation, Atmosphere. 13 (5) (2022) 770, https://doi.org/10.3390/atmos13050770.
[115] T.C. Hsiao, Y.C. Lee, K.C. Chen, W.C. Ye, K. Sopajaree, Y.I. Tsai, Experimental comparison of two portable and real-time size distribution analyzers for nano/submicron aerosol measurements, Aerosol Air Qual. Res. 16 (2016) 919–929, https://doi.org/10.4209/aaqr.2015.10.0614.
[116] T. Rönkkö, H. Kuuluvainen, P. Karjalainen, J. Keskinen, R. Hillamo, J.V. Niemi, L. Pirjola, H.J. Timonen, S. Saarikoski, E. Saukko, A. Järvinen, H. Silvennoinen, A. Rostedt, M. Olin, J. Yli-Ojanperä, P. Nousiainen, A. Kousa, M. Dal Maso, Traffic is a major source of atmospheric nanocluster aerosol, Proc. Natl. Acad. Sci. U.S.A. 114 (2017) 7549–7554, https://doi.org/10.1073/pnas.1700830114.
[117] E. Weingartner, C. Keller, W.A Stahel, H. Burtscher, U. Baltensperger, Aerosol emission in a road tunnel, Atmos. Environ. 31 (3) (1997) 451–462, https://doi.org/10.1016/S1352-2310(96)00193-8.

[118] D. Xu, H. Yu, W. Cai, J. Xu, J. Li, Primary particulate matter and aerosol emissions from biodiesel engines during idling in plateau environments of China, Sustainability. 17 (3) (2025) 976, https://doi.org/10.3390/su17030976.
[119] K. Teinilä, S. Saarikoski, H. Lintusaari, T. Lepistö, P. Marjanen, M. Aurela, H. Hellén, T. Tykkä, M. Lampimäki, J. Lampilahti, L. Barreira, T. Mäkelä, L. Kangas, J. Hatakka, S. Harni, J. Kuula, J.V. Niemi, H. Portin, J. Yli-Ojanperä, V. Niemelä, M. Jäppi, K. Lehtipalo, J. Vanhanen, L. Pirjola, H.E. Manninen, T. Petäjä, T. Rönkkö, H. Timonen, Measurement report: wintertime aerosol characterization at an urban traffic site in Helsinki, Finland, Atmos. Chem. Phys. 25 (2025) 4907–4928, https://doi.org/10.5194/acp-25-4907-2025.
[120] J.A. Lednicky, M. Lauzardo, M.M. Alam, M.A. Elbadry, C.J. Stephenson, J. C. Gibson, J.G. Morris, Isolation of SARS-CoV-2 from the air in a car driven by a COVID patient with mild illness, Int. J. Infectious Dis. 108 (2021) 212–216, https://doi.org/10.1016/j.ijid.2021.04.063.
[121] S.Nannu Shankar, C.T. Witanachchi, A.F. Morea, J.A. Lednicky, J.C. Loeb, M. M. Alam, Z.H. Fan, A. Eiguren-Fernandez, C.Y. Wu, SARS-CoV-2 in residential rooms of two self-isolating persons with COVID-19, J. Aerosol Sci. 159 (2022) 105870, https://doi.org/10.1016/j.jaerosci.2021.105870.
[122] C. Bi, J.P. Maestre, H. Li, G. Zhang, R. Givehchi, A. Mahdavi, K.A. Kinney, J. Siegel, S.D. Horner, Y. Xu, Phthalates and organophosphates in settled dust and HVAC filter dust of U.S. low-income homes: association with season, building characteristics, and childhood asthma, Environ. Int. 121 (2018) 916–930, https://doi.org/10.1016/j.envint.2018.09.013.
[123] Y. Wan, M.L. Diamond, J.A. Siegel, Quantitative filter forensics for semivolatile organic compounds in social housing apartments, Indoor Air. 32 (2) (2022) e12994, https://doi.org/10.1111/ina.12994.
[124] Z. Liu, Y. Deng, S. Ma, B.J. He, G. Cao, Dust accumulated fungi in air-conditioning system: findings based on field and laboratory experiments, Build. Simul. 14 (2021) 793–811, https://doi.org/10.1007/s12273-020-0693-3.
[125] W.J. Fisk, M. Spears, D.P. Sullivan, M. Mendell, Ozone removal by filters containing activated carbon: A pilot study. Proceedings of the Healthy Buildings 2009 Conference, Syracuse, NY, 2009.
[126] T. Ben-David, S. Wang, A. Rackes, M.S. Waring, Measuring the efficacy of HVAC particle filtration over a range of ventilation rates in an office building, Build. Environ. 144 (2018) 648–656, https://doi.org/10.1016/j.buildenv.2018.08.018.
[127] S.C. Chen, D.Q. Chang, C. Pei, C.J. Tsai, D.Y.H. Pui, Removal efficiency of bimodal $PM_{2.5}$ and PM_{10} by electret respirators and mechanical engine intake filters, Aerosol Air Qual. Res. 16 (2016) 1722–1729, https://doi.org/10.4209/aaqr.2015.08.0494.
[128] S. Jaganathan, H. Vahedi Tafreshi, B. Pourdeyhimi, On the pressure drop prediction of filter media composed of fibers with bimodal diameter distributions, Powder Technol. 181 (2008) 89–95, https://doi.org/10.1016/j.powtec.2007.07.002.
[129] C. Huang, B.E. Boor, Integration of a thermal aerosol generator into a full-scale HVAC filter test rig for aging filters with representative urban aerosol size distributions (RP-1734), Sci. Technol. Built Environ. 32 (2) (2026) 206–225, https://doi.org/10.1080/23744731.2025.2582421.
[130] ISO. 2024. Road vehicles—test contaminants for filter evaluation—part 1: Arizona test dust. 3rd ed. ISO 12103-1:2024. International Organization for Standardization. https://standards.iteh.ai/catalog/standards/iso/16cbf0b5-026b-4063-b616-6a03c18f3906/iso-12103-1-2024.
[131] C. Huang, N. Jung, B.E. Boor, A novel methodology for rapid aging of HVAC filters using a synthetic submicron aerosol: effects of HVAC system operational and environmental conditions on filter loading, Build. Environ. 286 (2025) 113564, https://doi.org/10.1016/j.buildenv.2025.113564.